

Electric-Field Control of Magnetic Anisotropies: Applications to Kitaev Spin Liquids and Topological Spin Textures

Shunsuke C. Furuya and Masahiro Sato

Department of Physics, Ibaraki University, Mito, Ibaraki 310-8512, Japan

(Dated: October 14, 2021)

Magnetic anisotropies originate from the spin-orbit coupling and determine the phase that magnetic systems fall into. We develop a microscopic theory for DC electric-field controls of magnetic anisotropies in magnetic Mott insulators and discuss its applications to Kitaev materials and topological spin textures. First, we derive a Kitaev-Heisenberg model based on a microscopic approach similar to that by G. Jackeli and G. Khaliullin, Phys. Rev. Lett. **102**, 017205 (2009). In the presence of a strong intra-atomic spin-orbit coupling, DC electric fields add non-Kitaev interactions such as a Dzyaloshinskii-Moriya interaction and an off-diagonal Γ' interaction to the Kitaev-Heisenberg model and can induce a topological quantum phase transition between Majorana Chern insulating phases. We also investigate the inter-atomic Rashba spin-orbit coupling and its effects on topological spin textures. DC electric fields turn out to create and annihilate magnetic skyrmions, hedgehogs, and chiral solitons.

Introduction.— The spin-orbit coupling (SOC) is of significance to topological electronic states of matters [1–6]. Recently, magnetic anisotropies, a direct descendent of SOC, has enjoyed renewed theoretical and experimental interests for their essential roles in topological states of magnetic materials such as topological spin textures (TST) [7, 8] and Kitaev spin liquids [9–13].

Violating an inversion symmetry, the SOC gives antisymmetric magnetic anisotropies also known as the Dzyaloshinskii-Moriya interaction (DMI) [14, 15]. Competitions between the DMI and ferromagnetic exchange interactions yield TST such as magnetic skyrmions [Figs. 1 (a) and (b)] [16–20], magnetic hedgehogs [21–24], and chiral solitons [Fig. 1 (c) and (d)] [25–27]. Carrying a nonzero topological index, TST is robust against thermal noises and other local disturbances. TST is thus promising for device applications [7, 8, 28].

The SOC also gives inversion-symmetric magnetic anisotropies that render the Kitaev material topological [9–13, 29–35]. The Kitaev model and its derivatives exhibit gapless and gapped quantum spin liquids (QSLs) [9, 13, 29–35], significant to fundamental physics and simultaneously relevant for quantum computation. In light of scientific interests and engineering applications, controlling methods of these SOC-driven topological states of magnetic materials are currently one of the central issues in condensed-matter physics, quantum physics, and applied physics [36–42].

The DC electric field holds promise for external controls of topological states of magnetic materials. As is well known, noncollinear magnetic orders of TSTs can drive the electric polarization [45–51]. For device applications, however, we need to create the TST even when we cannot expect the noncollinear magnetic order in the first place [e.g., the ferromagnetic state of Figs. 1 (b),(d)]. Controlling magnetic anisotropies will enable such a creation of the TST. The situation becomes even more non-trivial in Kitaev materials with no magnetic orders. On the other hand, recent technological advances such as electric double-layer transistors [52, 53] and interfacial en-

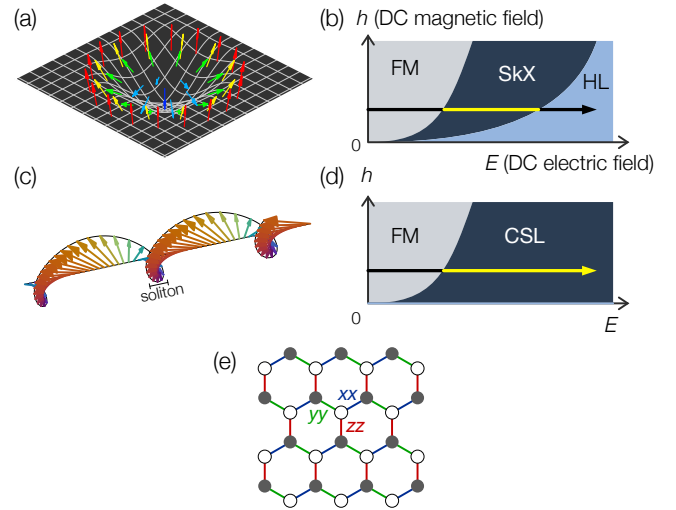


FIG. 1. (a) Néel-type magnetic skyrmion. (b) Schematic phase diagram of square-lattice classical Heisenberg ferromagnetic model with DMI (6), including helical (HL), Skyrmion-crystal (SkX), and ferromagnetic (FM) phases [16–18, 43, 44]. (c) Chiral soliton lattice (CSL) in spin chain. (d) Schematic phase diagram of classical Heisenberg ferromagnetic chain (7) with DMI, including HL, CSL, and FM phases [25–27]. (e) Kitaev model on honeycomb lattice.

gineerings [38, 54, 55] make strong DC electric fields of $\sim 1\text{--}10$ MV/cm available. Scanning tunneling microscopes can also yield DC electric fields of ~ 10 MV/cm locally [55–57]. To design materials and experiments, we need detailed information of how the external DC electric field changes microscopic parameters qualitatively and quantitatively [58, 59]. However, such a microscopic theory is not available yet for DC electric-field controls of magnetic anisotropies.

This Letter develops a microscopic quantum theory for DC electric-field controls of magnetic anisotropies in magnetic Mott insulators. We show how the DC electric field \mathbf{E} controls TSTs and Kitaev QSLs. We emphasize

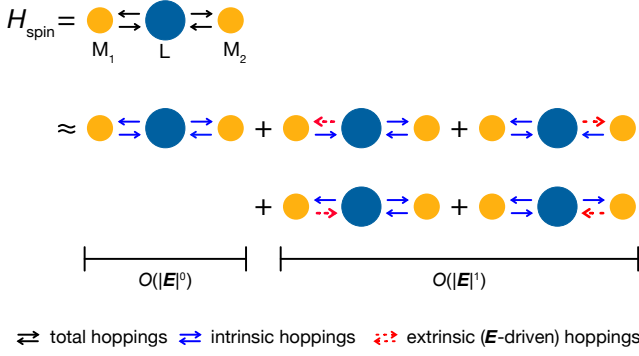


FIG. 2. Diagrammatic representation of spin Hamiltonian (1) with zeroth-order term omitted. The black solid, blue solid, and red dashed arrows denote the total hoppings $\mathcal{H}_t(\mathbf{E})$, the intrinsic hoppings $\mathcal{H}_t(\mathbf{0})$, and the extrinsic (\mathbf{E} -driven) hoppings $\delta\mathcal{H}_t$, respectively.

that our theory is generic and applicable to various magnetic systems beyond these specific examples.

Framework.— The spin Hamiltonian determining magnetic properties of Mott insulators originates from virtual hopping processes of electrons under strong interactions. These hopping processes are well described by Hubbard-like tight-binding models [15, 31, 59–63]. Considering the locality of virtual hopping processes in Mott insulating phase, we deal with models with three sites, two magnetic-ion sites (M_1 and M_2) with half-occupied d orbitals and a ligand site (L) with fully occupied p orbitals. We limit ourselves to $S = 1/2$ quantum spin systems with superexchange interactions mediated by p orbitals for simplicity. Note that we can treat the $S = 1/2$ spin and a $J_{\text{eff}} = 1/2$ pseudospin equally, as we see later.

The SOC and a crystal-electric field (CEF) lift the orbital degeneracy and define orbitals relevant to low-energy quantum spin systems. The SOC can generate spin-flipping electron hoppings intrinsically or otherwise extrinsically in collaboration with the DC electric field \mathbf{E} . Spin-flipping hoppings lead to magnetic anisotropies [15]. This Letter deals with microscopic Hubbard-like models with a generic Hamiltonian $\mathcal{H} = \mathcal{H}_U(\mathbf{E}) + \mathcal{H}_t(\mathbf{E})$, where $\mathcal{H}_U(\mathbf{E})$ and $\mathcal{H}_t(\mathbf{E})$ are intra-atomic and inter-atomic interactions under electric fields \mathbf{E} , respectively. $\mathcal{H}_t(\mathbf{0})$ denotes the intrinsic electron hoppings and the difference $\delta\mathcal{H}_t(\mathbf{E}) := \mathcal{H}_t(\mathbf{E}) - \mathcal{H}_t(\mathbf{0})$ contains extrinsic (\mathbf{E} -driven) hoppings.

We regard intrinsic and extrinsic hoppings $\mathcal{H}_t(\mathbf{E})$ as a perturbation to $\mathcal{H}_U(\mathbf{E})$. Performing the fourth-order perturbation expansion, we obtain the effective spin Hamiltonian [59],

$$\mathcal{H}_{\text{spin}} = P\mathcal{H}_U P + P\mathcal{H}_t \left(\frac{1}{E_g - \mathcal{H}_U} Q\mathcal{H}_t \right)^3 P, \quad (1)$$

where P is the projection operator to the Mott-insulating ground states of $\mathcal{H}_U(\mathbf{E})$ with the eigenenergy E_g and

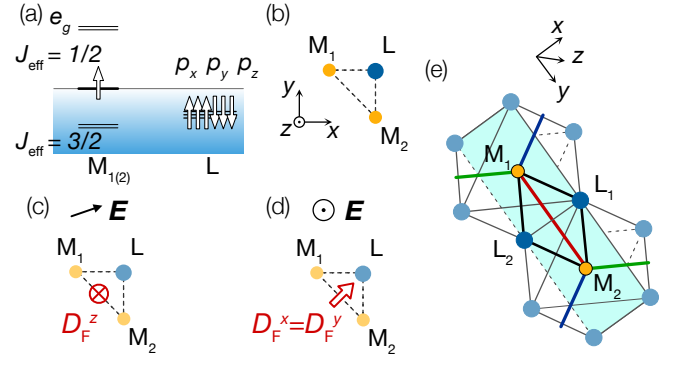


FIG. 3. (a) Half-occupied Γ_{7+} orbital ($J_{\text{eff}} = 1/2$ doublet) at M_j and fully occupied degenerate $p_{x,y,z}$ orbitals at ligand site (L). (b) Isosceles right triangle ΔM_1-L-M_2 . (c) Out-of-plane DMI in $J_{\text{eff}} = 1/2$ model driven by in-plane \mathbf{E} . (d) In-plane DMI in $J_{\text{eff}} = 1/2$ model driven by out-of-plane \mathbf{E} . DMI grows perpendicular to \mathbf{E} for both cases. Out-of-plane \mathbf{E} also generates the Γ' interaction. (e) Edge-sharing octahedra of ligands with $M_{1,2}$ at their centers, building block of Kitaev model [Fig. 1 (e)] [31]. When $\Delta M_1-L_1-M_2 \equiv \Delta M_1-L_2-M_2$, the M_1-M_2 bond has the spin Hamiltonian (4) is *not* parallel to the xy plane spanned by the $M_{1,2}$ and $L_{1,2}$ sites (the light blue rectangle) because DMI from the $M_1-L_n-M_2$ paths cancel each other out.

$Q = 1 - P$ is to its complementary space. The zeroth-order term $P\mathcal{H}_U(\mathbf{E})P$ is mostly irrelevant but gives the uniform Zeeman energy, $P\mathcal{H}_U P = -\sum_{a=x,y,z} \sum_j h^a S_j^a$ with $\mathbf{h} = \mathbf{g}\mathbf{B}$ for the magnetic field $\mathbf{B} = \mu_0\mathbf{H}$ [59], where \mathbf{g} is the electron's g tensor. Hereafter, we call \mathbf{h} the magnetic field for simplicity. The fourth-order process gives the ligand-mediated superexchange interaction.

Figure 2 shows a diagrammatic representation of the fourth-order process in Eq. (1). The black, blue, and red arrows represent the total hoppings $\mathcal{H}_t(\mathbf{E})$, the intrinsic ones $\mathcal{H}_t(\mathbf{0})$, and the extrinsic ones, $\delta\mathcal{H}_t(\mathbf{E})$, respectively. The intrinsic $O(|\mathbf{E}|^0)$ diagram typically contains the Heisenberg superexchange interaction [59, 60]. We obtain the intrinsic superexchange interaction from the diagram with the four blue arrows. Hopping amplitudes of the extrinsic (\mathbf{E} -driven) hoppings are $O(|\mathbf{E}|)$, as we show below. We obtain the $O(|\mathbf{E}|)$ correction to the spin Hamiltonian from diagrams with three blue and one red arrows. This $|\mathbf{E}|$ -linear approximation works even under (currently feasible) strong electric fields regardless of whether the field is extrinsic or comes from interfacial electric fields.

Kitaev-Heisenberg model.— Based on the generic framework, we discuss Kitaev materials. We consider a low-spin d^5 electron configuration under the octahedral CEF and the strong SOC [31], where the $J_{\text{eff}} = 1/2$ doublet hosts the $J_{\text{eff}} = 1/2$ (pseudo)spin [Fig. 3 (a)]. The $J_{\text{eff}} = 1/2$ state is a spin-orbit-entangled superposition of t_{2g} states, $|\uparrow, l^z = 0\rangle$ and $|\downarrow, l^z = 1\rangle$ [31, 64–67]. Here, we assume an isosceles right triangle ΔM_1-L-M_2 formed on the xy plane [Fig. 3 (b)]. The intrinsic hoppings

between M_j and L involve with t_{2g} and $p_{x,y,z}$ orbitals: $\mathcal{H}_t(\mathbf{0}) = t \sum_{\sigma=\pm} (p_{y,\sigma}^\dagger d_{1,xy,\sigma} + p_{z,\sigma}^\dagger d_{1,zx,\sigma} + p_{x,\sigma}^\dagger d_{2,xy,\sigma} + p_{z,\sigma}^\dagger d_{2,yz,\sigma} + \text{H.c.})$. Note that the t_{2g} orbitals are reconstructed in the spin-orbit-entangled way. We can rewrite t_{2g} -orbital creation and annihilation operators by those ($d_{j,\Gamma_{7+},\sigma}$ and $d_{j,\Gamma_{7+},\sigma}^\dagger$) of the $J_{\text{eff}} = 1/2$ doublets [55]:

$$\mathcal{H}_t(\mathbf{0}) = \frac{t}{\sqrt{3}} \sum_{\sigma=\pm} [(p_{y,\sigma}^\dagger + ip_{z,-\sigma}^\dagger) d_{1,\Gamma_{7+},\sigma} + (p_{x,\sigma}^\dagger + \sigma p_{y,-\sigma}^\dagger) d_{2,\Gamma_{7+},\sigma} + \text{H.c.}] \quad (2)$$

Here, Γ_{7+} labels the irreducible representation of the $J_{\text{eff}} = 1/2$ doublet [64, 66].

The intrinsic hoppings (2) lead to the following spin Hamiltonian,

$$\mathcal{H}_{\text{spin}}(\mathbf{0}) = J_{\text{F}} \mathbf{S}_1 \cdot \mathbf{S}_2 + K S_1^z S_2^z - \sum_{a=x,y,z} \sum_{j=1,2} h^a S_j^a \quad (3)$$

with $J_{\text{F}} = -\frac{8}{3} t^4 \frac{1}{(U_d - U_p + \Delta_{dp})^2} \frac{1}{2(U_d - U_p + \Delta_{dp}) - J_{\text{H}}} < 0$ and $K = -2J_{\text{F}} > 0$. Here, $U_{d,p}$, J_{H} , and $\Delta_{dp} = E_d - E_p$ are microscopic parameters of \mathcal{H}_U and denote the on-site Coulomb repulsion of d, p orbitals, the p -orbital Coulomb exchange, and the d -orbital eigenenergy (E_d) relative to the p -orbital one (E_p), respectively [55].

Following the argument of Ref. [31], we can build the Kitaev-Heisenberg model on the honeycomb lattice from our model (3) [55]. Note that we found the Kitaev and Heisenberg interactions coexistent in Eq. (3) unlike Ref. [31]. This discrepancy is partly attributed to details of $\mathcal{H}_U(\mathbf{E})$. The ferromagnetic superexchange $J_{\text{F}} < 0$ accords with a universal law, the Goodenough-Kanamori rule [68–70]. By contrast, the antiferromagnetic Kitaev coupling $K > 0$ is less universal, and arises from a specificity of our model. Including direct overlaps of the Γ_{7+} orbitals at M_1 and M_2 turns the Kitaev coupling K ferromagnetic [62].

We now give our attention to \mathbf{E} -driven interactions absent in the model (3) on the xy plane. In-plane and out-of-plane electric fields yield different hopping processes. The in-plane electric field yields hoppings, $\delta\mathcal{H}_t(\mathbf{E}) = -I \sum_{\sigma=\pm} \{E^y (p_{z,\sigma}^\dagger d_{1,yz,\sigma} + p_{x,\sigma}^\dagger d_{1,xy,\sigma} + \text{H.c.}) + E^x (p_{z,\sigma}^\dagger d_{2,zx,\sigma} + p_{y,\sigma}^\dagger d_{2,xy,\sigma} + \text{H.c.})\}$, keeping a reflection symmetry about the xy plane, $(x, y, z) \rightarrow (x, y, -z)$. The factor $I = e \int d\mathbf{r} \langle p_{x,\sigma} | \mathbf{r} \rangle y \langle \mathbf{r} | d_{j,xy,\sigma} \rangle$ is a constant with the dimension of the electric polarization [55]. Let us replace the t_{2g} -orbital operators in $\delta\mathcal{H}_t(\mathbf{E})$ by the Γ_{7+} ones as we did for $\mathcal{H}_t(\mathbf{0})$. The reflection symmetry about the xy plane permits the DMI with the nonzero z component [Fig. 3 (c)]. Explicit calculations of Eq. (1) show that the in-plane electric field adds $\mathbf{D}_{\text{F}} \cdot \mathbf{S}_1 \times \mathbf{S}_2 = D_{\text{F}}^z (\mathbf{S}_1 \times \mathbf{S}_2)^z$ with $\frac{D_{\text{F}}^z}{J_{\text{F}}} = -\frac{4I}{t} \frac{(E^x + E^y)(U_d - U_p + \Delta_{dp}) + (E^x - E^y)J_{\text{H}}}{2(U_d - U_p) + J_{\text{H}}}$ to the Kitaev-Heisenberg Hamiltonian (3) in accordance with the reflection symmetry [55].

The out-of-plane electric field $\mathbf{E} = E^z \mathbf{e}_z$ violates the reflection symmetry about the xy plane but keeps another reflection symmetry, $(x, y, z) \rightarrow (y, x, z)$, about a

plane $\mathcal{M} := \{(x, y, z) | x = y\}$ perpendicular to the M_1 – M_2 bond. This reflection symmetry confines the DMI vector \mathbf{D}_{F} to the intersection of the \mathcal{M} plane and the xy plane. Straightforward calculations give

$$\mathcal{H}_{\text{spin}} = J_{\text{F}} \mathbf{S}_1 \cdot \mathbf{S}_2 + K S_1^z S_2^z - \sum_{a=x,y,z} \sum_{j=1,2} h^a S_j^a + \mathbf{D}_{\text{F}} \cdot (\mathbf{S}_1 \times \mathbf{S}_2) + \Gamma' [(S_1^x + S_1^y) S_2^z + S_1^z (S_2^x + S_2^y)], \quad (4)$$

$$\text{with } \mathbf{D}_{\text{F}} = D_{\text{F}}^x (\mathbf{e}_x + \mathbf{e}_y), \quad D_{\text{F}}^x = \frac{16t^3}{3} E^z I \left(\frac{1}{U_d - U_p + \Delta_{dp}} \right)^2 \frac{J_{\text{H}}}{4(U_d - U_p + \Delta_{dp})^2 - J_{\text{H}}^2}, \quad \text{and} \\ \Gamma' = \frac{32t^3}{9} E^z I \left(\frac{1}{U_d - U_p + \Delta_{dp}} \right)^2 \frac{U_d - U_p + \Delta_{dp}}{4(U_d - U_p + \Delta_{dp})^2 - J_{\text{H}}^2} \quad [55].$$

The out-of-plane electric field also drives the symmetric off-diagonal magnetic anisotropy, $\Gamma'(S_1^y S_2^z + S_1^z S_2^y)$, known as the Γ' interaction [71, 72] in the context of Kitaev materials. Both the DMI and the Γ' interaction accord with the reflection symmetry about \mathcal{M} .

Gapped QSL.— The Kitaev-Heisenberg-DMI- Γ' Hamiltonian built from Eq. (4) guides us to experimental controls of Kitaev materials. Currently, much effort is being made to investigate effects of non-Kitaev interactions on QSL states of the pure Kitaev model because non-Kitaev interactions are present in real Kitaev materials such as α -RuCl₃ [73–80].

The Kitaev model can have a gapped QSL phase with the Chern number $C = 1$ when $h^x h^y h^z \neq 0$ [29]. The Majorana mass gap $\propto |h^x h^y h^z|$ is the third order of the external magnetic field. Interestingly, the Γ' interaction generates the mass $\propto |h^x \Gamma'|$ of the Majorana fermion together with the magnetic field [71, 72]. If $\Gamma' = 0$ for $\mathbf{E} = \mathbf{0}$, the Majorana mass $\propto |h^x E^z|$ is the second order about the external electromagnetic fields. The \mathbf{E} -driven Γ' interaction can induce quantum phase transitions between gapped QSLs with different Chern numbers [72]. A recent study [81] pointed out that the DMI can also drive quantum phase transitions between gapped QSLs under magnetic fields. The electric field controls these magnetic anisotropies and drives topological quantum phase transitions under a constant magnetic field.

The DMI sustains when we build the Kitaev-Heisenberg-DMI- Γ' model from our three-site model (4) [Figs. 1 (e) and 3 (e)] if the L_1 and L_2 sites are crystallographically nonequivalent. The inversion-symmetric Γ' interaction sustains even when L_1 and L_2 are equivalent. For example, we obtain the Kitaev-Heisenberg- Γ' model when we apply the electric field along, for example, the [111] direction [55]. We may expect topological phase transitions due to the \mathbf{E} -driven DMI and the \mathbf{E} -driven Γ' interaction if a Kitaev material is close enough to the transition point in the $\mathbf{h} - \Gamma'$ phase diagram.

For α -RuCl₃, we can use parameters $U_d = 2.5$ meV, $U_p = 1.5$ meV, $\Delta_{dp} = 5.5$ meV, $J_{\text{H}} = 0.7$ meV, and $t = 0.5$ meV [80]. These parameters give $J_{\text{F}} = -3$ meV and $K = -2J_{\text{F}}$. As we mentioned, our model gives antiferromagnetic $K > 0$ but can make it ferromagnetic $K < 0$ with slight modifications of the model. If we ignore the \mathbf{E} dependence of J_{F} as we did thus far in

this Letter, we find that a DC electric field 1–10 MV/cm change $|D_{\text{F}}^x|$ and $|\Gamma'|$ only by 10^{-4} – 10^{-3} % of J_{F} , which is too much underestimated. Note that the 1–10 MV/cm DC electric field can reduce J_{F} by 1–10 % [59]. This reduction enhances the change in the ratios $|D_{\text{F}}^x/J_{\text{F}}|$ and $|\Gamma'/J_{\text{F}}|$. We can further enhance the DC electric-field effect, by including Rashba-SOC-driven hoppings besides the hitherto considered intra-atomic SOC.

Rashba spin-orbit coupling.— We can effectively regard that the single-electron Hamiltonian \hat{H}_1 contains the Rashba SOC, namely, $-\alpha_{\text{R}}(\boldsymbol{\sigma} \times \mathbf{k}) \cdot \mathbf{e}(\mathbf{r})$, where \mathbf{k} is the wavevector of the electron in the crystal and $\mathbf{e}(\mathbf{r}) = \mathbf{E}(\mathbf{r})/|\mathbf{E}(\mathbf{r})|$ is the unit vector parallel to the electric field $\mathbf{E}(\mathbf{r})$. We can deem $\mathbf{E}(\mathbf{r})$ the external electric field, a surface electric field for thin-film materials [82, 83], or an interfacial electric field for field-effect transistors [52, 53]. The coefficient α_{R} is proportional to $|\mathbf{E}(\mathbf{r})|$. The Rashba SOC affects the single-electron Hamiltonian and turns into spin-flipping hoppings and eventually into the DMI.

For demonstration, we again consider the isosceles right triangle of Fig. 3 (b). We also inherit the electron configuration, the low-spin d^5 configuration under the octahedral CEF. The only difference from the previous $J_{\text{eff}} = 1/2$ model lies in SOC mechanisms. This time, we consider Rashba-SOC-driven hoppings but ignore the d -orbital splitting due to the SOC. Given that the d_{xy} orbital carries the $S = 1/2$ spin, we find $\mathcal{H}_t(\mathbf{0}) = t \sum_{\sigma} (p_{y,\sigma}^\dagger d_{1,xy,\sigma} + p_{x,\sigma}^\dagger d_{2,xy,\sigma} + \text{H.c.})$. The superexchange interaction is again ferromagnetic: $\mathcal{H}_{\text{spin}}(\mathbf{0}) = J_{\text{R}} \mathbf{S}_1 \cdot \mathbf{S}_2$ with $J_{\text{R}} = -8t^2 \frac{J_{\text{H}}}{4(U_d - U_p + \Delta_{dp})^2 - J_{\text{H}}^2} (\frac{1}{U_d - U_p + \Delta_{dp}})^2 < 0$ [59].

The Rashba SOC due to the out-of-plane electric field $\mathbf{E} = E^z \mathbf{e}_z$ gives [1, 2]

$$\delta\mathcal{H}_t(\mathbf{E}) = \sum_{s,s'} [i\lambda p_{y,s}^\dagger (\boldsymbol{\sigma}^{ss'} \times \mathbf{d}_1)^z d_{1,xy,s'} + i\lambda p_{x,\sigma}^\dagger (\boldsymbol{\sigma}^{ss'} \times \mathbf{d}_2)^z d_{2,xy,s'} + \text{H.c.}], \quad (5)$$

with a unit vector \mathbf{d}_j pointing toward the ligand site from M_j . The hopping amplitude λ equals to $\alpha_{\text{R}}|\mathbf{k}|$. The extrinsic hoppings (5) yield the in-plane DMI $\mathbf{D}_{\text{R}} \cdot \mathbf{S}_1 \times \mathbf{S}_2$ with $\mathbf{D}_{\text{R}} = D_{\text{R}}^x \mathbf{e}_x + D_{\text{R}}^y \mathbf{e}_y$ and $D_{\text{R}}^x = -16\lambda t^3 (\frac{1}{U_d - U_p + \Delta_{dp}})^2 \frac{U_d - U_p + \Delta_{dp}}{4(U_d - U_p + \Delta_{dp})^2 - J_{\text{H}}^2}$ and $D_{\text{R}}^y = -16\lambda t^3 (\frac{1}{U_d - U_p + \Delta_{dp}})^2 \frac{J_{\text{H}}}{4(U_d - U_p + \Delta_{dp})^2 - J_{\text{H}}^2}$. Note that the DMI violates the inversion symmetry about the \mathcal{M} plane because the Rashba SOC $-\alpha_{\text{R}}(\boldsymbol{\sigma} \times \mathbf{k})^z$ does.

For a parameter set $U_d = 3$ meV, $U_p = 2$ meV, $\Delta_{dp} = 5$ meV, $J_{\text{H}} = 1$ meV, $t = 0.1$ meV, and $\lambda = 0.05$ meV, we obtain $|D_{\text{R}}^x/J_{\text{R}}| \approx 0.46$. We used a value $\lambda = 0.05$ meV, much smaller than $\lambda = \alpha_{\text{R}}|\mathbf{k}| \propto |\mathbf{E}(\mathbf{r})|$ estimated in some materials [84, 85]. Because α_{R} is well controllable with the electric field [85], we may expect that the external DC electric field can control the DMI substantially both for Kitaev spin liquids and TSTs.

Magnetic skyrmion lattice.— We can directly apply our Rashba SOC argument to controls of magnetic skyrmion

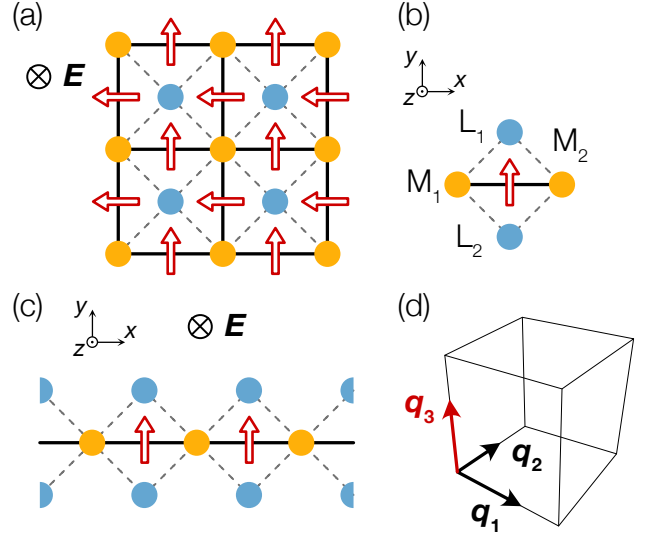


FIG. 4. (a) Edge-sharing octahedra ML_4 projected to xy plane. Magnetic ions form the square lattice (black solid lines). Intrinsic and extrinsic hoppings occur on dashed gray bonds. (b) Four-site model for nearest-neighbor superexchange interaction of magnetic ions. (c) Smallest square plaquette of resultant spin model (6). (d) One-dimensional version of square-lattice model (a), ferromagnetic spin chain with uniform DMI. (e) \mathbf{q} vectors of $3\mathbf{q}$ -hedgehog state [8, 24, 86].

lattice [16–18, 43, 44]. We exemplify this application by considering a two-dimensional array of edge-sharing octahedra whose centers have magnetic ions and vertices have ligand ions [Fig. 4 (a)]. The magnetic ions form the square lattice on the xy plane. We can build this many-body model with the small square plaquette of Fig. 4 (b) made of two isosceles right triangles $\triangle M_1-L_1-M_2$ and $\triangle M_1-L_2-M_2$. Assuming the Rashba SOC (5) on the $M_j-L_{j'}$ bonds, we obtain the spin Hamiltonian for the building block of Fig. 4 (b): $\mathcal{H}_{\text{spin}} = J_{\text{R}} \mathbf{S}_1 \cdot \mathbf{S}_2 + D_{\perp} \mathbf{e}_{\perp} \cdot (\mathbf{S}_1 \times \mathbf{S}_2) - h_z \sum_j S_j^z$, where we applied both the electric and magnetic fields parallel to the z axis. The vector $D_{\perp} \mathbf{e}_{\perp}$ with $D_{\perp} = \sqrt{2}(D_{\text{R}}^x + D_{\text{R}}^y)$ is depicted as the red-fringe arrow in Figs. 4 (a), (b), and (c). With many square plaquettes of Fig. 4 (b), we can build a square-lattice ferromagnet [Fig. 4 (a)],

$$\begin{aligned} \mathcal{H}_{\text{SkX}} = & -|J_{\text{R}}| \sum_{\mathbf{r}} (\mathbf{S}_{\mathbf{r}} \cdot \mathbf{S}_{\mathbf{r}+\mathbf{e}_x} + \mathbf{S}_{\mathbf{r}} \cdot \mathbf{S}_{\mathbf{r}+\mathbf{e}_y}) - h^z \sum_{\mathbf{r}} S_{\mathbf{r}}^z \\ & + D_{\perp}(E^z) \sum_{\mathbf{r}} (\mathbf{S}_{\mathbf{r}} \times \mathbf{S}_{\mathbf{r}+\mathbf{e}_x} \cdot \mathbf{e}_y - \mathbf{S}_{\mathbf{r}} \times \mathbf{S}_{\mathbf{r}+\mathbf{e}_y} \cdot \mathbf{e}_x). \end{aligned} \quad (6)$$

The model (6) realizes the Néel-type magnetic skyrmion lattice because a 90° rotation $(S_{\mathbf{r}}^x, S_{\mathbf{r}}^y, S_{\mathbf{r}}^z) \rightarrow (-S_{\mathbf{r}}^y, S_{\mathbf{r}}^x, S_{\mathbf{r}}^z)$ turns the model (6) into a model that exhibits the Bloch-type skyrmion lattice [43]. The out-of-plane electric field thus controls the ratio $D_{\perp}(E^z)/J_{\text{R}}(E^z)$ [Fig. 1 (b)] and allows us to create and annihilate the skyrmion.

Chiral soliton lattice.— Building the ML_2 chain [Fig. 4 (c)] with the same square plaquette, we can construct a ferromagnetic chain,

$$\mathcal{H}_{\text{CSL}} = -|J_{\text{R}}| \sum_j \mathbf{S}_j \cdot \mathbf{S}_{j+1} - D_{\perp}(E^z) \sum_j (\mathbf{S}_j \times \mathbf{S}_{j+1})^y - h^y \sum_j S_j^y, \quad (7)$$

which is nothing but the one-dimensional version of the model (6). The ferromagnetic chain (7) yields a topological spin texture, the CSL. The ML_2 chain is typically realized for $(M, L) = (\text{Cu}, \text{O})$. The electric field controls the ratio $D_{\perp}(E^z)/J_{\text{R}}(E^z)$ and turns the ferromagnetic state into the CSL [Fig. 1 (d)] [25–27].

Magnetic hedgehog lattice.— The Rashba SOC is appropriate to drive the chiral structure in a certain direction by generating a uniform DMI. This feature of the Rashba SOC will also be useful for multiple- \mathbf{q} states. Provided that a magnetic material shows a double- \mathbf{q} state with the two \mathbf{q} vectors lying on the q_x - q_y plane [\mathbf{q}_1 and \mathbf{q}_2 of Fig. 4 (e)] and the electric field \mathbf{E} adds another \mathbf{q} vector (\mathbf{q}_3). This feature of the electric field will drive the

magnetic hedgehog lattice where the triple- or quadruple- \mathbf{q} spin texture is required [8, 24, 86].

Summary and discussions.— This Letter discussed DC electric-field controls of Kitaev materials and TSTs. However, our theoretical framework is widely applicable to various other situations. For reference, we discuss an antiferromagnetic model with a d^9 electron configuration and weak intra-atomic SOC within p orbitals in the supplemental material [55].

Together with our previous works on DC electric-field controls of superexchange interactions [58, 59], this Letter provides the general theoretical foundation to DC electric-field controls of magnetism [36–38, 87–93], which takes on a growing importance with ongoing advances in strong DC electric-field source [36, 37, 52, 53], including a single-cycle terahertz laser pulse [94–99].

Acknowledgments.— The authors are grateful to Tet-suo Hanaguri for fruitful discussions. S.C.F. and M.S. are supported by a Grant-in-Aid for Scientific Research on Innovative Areas “Quantum Liquid Crystals” (Grant No. JP19H05825). M.S. is also supported by JSPS KAKENHI (Grant No. 20H01830)

Supplemental Material for “Electric-Field Control of Magnetic Anisotropies: Applications to Kitaev Spin Liquids and Topological Spin Textures”

Shunsuke C. Furuya and Masahiro Sato

Department of Physics, Ibaraki University, Mito, Ibaraki 310-8512, Japan

S1. FIELD-INDUCED MAGNETIC ANISOTROPIES IN KITAEV-HEISENBERG MODEL

A. Model at zero electric fields

In this Section, we derive the spin Hamiltonian of the $J_{\text{eff}} = 1/2$ model [Figs. S1 (a) and (b)]. The $J_{\text{eff}} = 1/2$ doublet at M_j are a spin-orbit-entangled superposition of t_{2g} orbitals. The up state ($|+\rangle_j$) and the down state ($|-\rangle_j$) state of the (pseudo)spin at M_j are given by

$$|+\rangle_j = \frac{1}{\sqrt{3}}(|d_{j,xy,\uparrow}\rangle + |d_{j,yz,\downarrow}\rangle + i|d_{j,zx,\downarrow}\rangle), \quad (\text{S1.1})$$

$$|-\rangle_j = \frac{1}{\sqrt{3}}(|d_{j,xy,\downarrow}\rangle - |d_{j,yz,\uparrow}\rangle + i|d_{j,zx,\uparrow}\rangle), \quad (\text{S1.2})$$

where $|d_{j,a,\sigma}\rangle = d_{j,a,\sigma}^\dagger |0\rangle$ is a spin- σ state of the d_a -orbital electron at M_j and $|0\rangle$ is the vacuum of the creation operator $d_{j,a,\sigma}^\dagger$. This doublet is labeled as Γ_{7+} using the Bethe’s notation of the double group [66]. Hereafter, we denote $\sigma = \uparrow, \downarrow$ as $\sigma = +, -$, respectively.

It is straightforward to write the intrinsic hoppings $\mathcal{H}_t(\mathbf{0})$ in terms of t_{2g} -orbital operators. As Figs. S1 (c) and (d) show, the electron in the p_y orbital can hop directly to the d_{xy} orbital at M_1 but cannot to that at M_2 because the d_{xy} orbital has the odd parity about a reflection $(x, y, z) \rightarrow (x, -y, z)$ but the p_y orbital has the even parity. Likewise, the electron in the p_x orbital can hop directly to the d_{xy} orbital at M_2 but cannot to that at M_1 because of the difference in the parity about another reflection $(x, y, z) \rightarrow (-x, y, z)$. Such crystalline symmetries permits the following intrinsic hoppings at $\mathbf{E} = \mathbf{0}$:

$$\mathcal{H}_t(\mathbf{0}) = t \sum_{\sigma=\pm} (p_{y,\sigma}^\dagger d_{1,xy,\sigma} + p_{z,\sigma}^\dagger d_{1,zx,\sigma} + p_{x,\sigma}^\dagger d_{2,xy,\sigma} + p_{z,\sigma}^\dagger d_{2,zx,\sigma} + \text{H.c.}). \quad (\text{S1.3})$$

The creation and annihilation operators of the t_{2g} -orbital electrons depend on each other in the $J_{\text{eff}} = 1/2$ model because they are spin-orbit entangled in the $J_{\text{eff}} = 1/2$ doublet. Here, we note that the orbital angular momentum $\mathbf{L} = -\mathbf{l}_d$ and the spin,

$$\mathbf{S}_d := \frac{\hbar}{2} \sum_{a=xy,yz,zx} \sum_{s,s'=\pm} d_{j,a,s}^\dagger \boldsymbol{\sigma}^{ss'} d_{j,a,s'}, \quad (\text{S1.4})$$

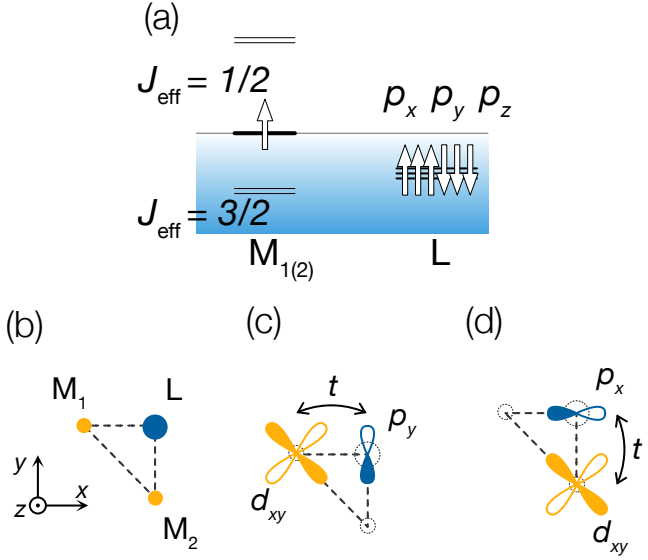


FIG. S1. (a) $J_{\text{eff}} = 1/2$ model's electron configurations in Γ_{7+} orbitals and $p_{x,y,z}$ orbitals at M_j and L sites. (b) Geometrical configuration of three sites, $M_{1,2}$ and L . $\triangle M_1-L-M_2$ forms a right-angle isosceles triangle. (c) Electron hopping between d_{xy} orbital at M_1 and p_y orbital at L . (d) Electron hopping between d_{xy} orbital at M_2 and p_x orbital at L . The hopping between d_{xy} at M_1 (M_2) and p_x (p_y) orbital at L is forbidden by symmetries.

form the effective total angular momentum \mathbf{J}_{eff} as follows [67].

$$\mathbf{J}_{\text{eff}} = -\mathbf{l}_d + \mathbf{S}_d. \quad (\text{S1.5})$$

Hereafter, we set $\hbar = 1$ for simplicity. \mathbf{S}_d and \mathbf{L} of the Γ_{7+} doublet are antiparallel to each other because electrons in the d^5 configuration feel the strong SOC $\xi \mathbf{L} \cdot \mathbf{S}_d$ with large positive ξ [67]. We can easily confirm

$$J_{\text{eff}}^z |\pm\rangle_j = \pm \frac{1}{2} |\pm\rangle_j. \quad (\text{S1.6})$$

Since there are few possibilities of confusions, we simply represent this pseudospin \mathbf{J}_{eff} as \mathbf{S}_j and call it a spin, as we did in the main text. The spin operator \mathbf{S}_j is thus defined as

$$S_j^z = \frac{1}{2} (|+\rangle_{jj} \langle +| - |-\rangle_{jj} \langle -|), \quad (\text{S1.7})$$

$$S_j^\pm = |\pm\rangle_{jj} \langle \mp|. \quad (\text{S1.8})$$

Our purpose in this subsection is to write the spin Hamiltonian in terms of this spin operator \mathbf{S}_j . For this purpose, we represent creation and annihilation operators of the t_{2g} orbitals in terms of the $J_{\text{eff}} = 1/2$ doublet, $d_{j,\Gamma_{7+},\sigma}^\dagger$ and $d_{j,\Gamma_{7+},\sigma}$. They are defined as

$$|+\rangle_j =: d_{j,\Gamma_{7+},+}^\dagger |0\rangle, \quad |-\rangle_j =: d_{j,\Gamma_{7+},-}^\dagger |0\rangle. \quad (\text{S1.9})$$

An operator, $n_{j,\Gamma_{7+},\sigma} = d_{j,\Gamma_{7+},\sigma}^\dagger d_{j,\Gamma_{7+},\sigma}$, counts the number of electrons with the σ spin in the Γ_{7+} doublet. We can relate t_{2g} -orbital operators $d_{j,a,\sigma}$ with $a = xy, yz, zx$ to the Γ_{7+} -orbital operator $d_{j,\Gamma_{7+},\sigma}$ as follows. For example, the operator $d_{j,xy,\sigma}$ satisfies

$$d_{j,xy,+} |\sigma\rangle_j = \frac{1}{\sqrt{3}} \delta_{\sigma,+} |0\rangle, \quad d_{j,xy,-} |\sigma\rangle_j = \frac{1}{\sqrt{3}} \delta_{\sigma,-} |0\rangle, \quad (\text{S1.10})$$

where $\delta_{a,b}$ is Kronecker's delta. These relations indicate

$$d_{j,xy,\sigma} P = Q d_{j,xy,\sigma} P = Q \left(\frac{1}{\sqrt{3}} d_{j,\sigma} \right) P, \quad (\text{S1.11})$$

at low energies, where $P = \bigotimes_{j=1,2} (|+\rangle_{jj} \langle +| + |-\rangle_{jj} \langle -|)$ is the projection operator to the Hilbert subspace spanned by the Γ_{7+} doublets and $Q = 1 - P$ is the projection to its complementary. Note a simple relation $P d_{j,a,\sigma} P = 0$ for $a = xy, yz, zx$. Likewise, we obtain

$$d_{j,yz,\sigma} P = Q d_{j,yz,\sigma} P = Q \left(-\frac{1}{\sqrt{3}} \sigma d_{j,-\sigma} \right) P, \quad (\text{S1.12})$$

$$d_{j,zx,\sigma} P = Q d_{j,zx,\sigma} P = Q \left(i \frac{1}{\sqrt{3}} d_{j,-\sigma} \right) P. \quad (\text{S1.13})$$

These relations lead to

$$\mathcal{H}_t(\mathbf{0}) P = \left\{ \frac{t}{\sqrt{3}} \sum_{\sigma=\pm} [(p_{y,\sigma}^\dagger + ip_{z,-\sigma}^\dagger) d_{1,\Gamma_{7+},\sigma} + (p_{x,\sigma}^\dagger + \sigma p_{y,-\sigma}^\dagger) d_{2,\Gamma_{7+},\sigma} + \text{H.c.}] \right\} P, \quad (\text{S1.14})$$

$$P \mathcal{H}_t(\mathbf{0}) = P \left\{ \frac{t}{\sqrt{3}} \sum_{\sigma=\pm} [(p_{y,\sigma}^\dagger + ip_{z,-\sigma}^\dagger) d_{1,\Gamma_{7+},\sigma} + (p_{x,\sigma}^\dagger + \sigma p_{y,-\sigma}^\dagger) d_{2,\Gamma_{7+},\sigma} + \text{H.c.}] \right\}. \quad (\text{S1.15})$$

At low energies, we can abbreviate these relations as Eq. (2) in the main text.

We are now ready to write down the many-body Hamiltonian

$$\mathcal{H} = \mathcal{H}_U + \mathcal{H}_t(\mathbf{0}), \quad (\text{S1.16})$$

of the the $J_{\text{eff}} = 1/2$ model at $\mathbf{E} = \mathbf{0}$. The intrinsic hoppings and the intra-atomic interactions \mathcal{H}_U are given by Eq. (2) and

$$\begin{aligned} \mathcal{H}_U = & U_d \sum_{j=1,2} n_{j,\Gamma_{7+},+} n_{j,\Gamma_{7+},-} + U_p \sum_{\mu=x,y,z} n_{p_\mu,+} n_{p_\mu,-} \\ & + \sum_{j=1,2} V_j \sum_{\sigma=\pm} n_{j,\sigma} + V_p \sum_{\sigma=\pm} \sum_{\mu=x,y,z} n_{p_\mu,\sigma} \\ & - J_H \sum_{\mu \neq \mu'} \mathbf{s}_\mu \cdot \mathbf{s}_{\mu'} - \sum_{j=1,2} \sum_{a=x,y,z} h^a S_j^a, \end{aligned} \quad (\text{S1.17})$$

respectively. Here, $n_{p_{\mu,\sigma}} := p_{\mu,\sigma}^\dagger p_{\mu,\sigma}$ is the number operator of the p_{μ} -orbital electron. U_d and U_p denote the intra-band Coulomb repulsions for the d and p orbitals, V_j and V_p are the on-site potentials at M_j and L , and $J_H > 0$ is the ferromagnetic direct exchange between

spins \mathbf{s}_{μ} in the p_{μ} orbitals.

B. Spin Hamiltonian at zero electric fields

Using the intrinsic hoppings (2) as a perturbation to Eq. (S1.17), we can derive the spin Hamiltonian (1),

$$\mathcal{H}_{\text{spin}} = P \left[-\frac{2}{9} t^4 \left(\frac{1}{U_d - U_p + V_1 - V_p} + \frac{1}{U_d - U_p + V_2 - V_p} \right)^2 \frac{1}{2(U_d - U_p) + V_1 + V_2 - 2V_p - J_H} (\mathbf{S}_1 \cdot \mathbf{S}_2 - 2S_1^z S_2^z) - \sum_{a=x,y,z} \sum_{j=1,2} h^a S_j^a \right] P + \text{const.} \quad (\text{S1.18})$$

Provided that $V_1 = V_2$, the spin Hamiltonian becomes the Kitaev-Heisenberg-like one (3) with

$$J_F = -\frac{8}{9} t^4 \left(\frac{1}{U_d - U_p + \Delta_{dp}} \right)^2 \frac{1}{2(U_d - U_p + \Delta_{dp}) - J_H}, \quad (\text{S1.19})$$

$$K = -2J_F, \quad (\text{S1.20})$$

where $\Delta_{dp} = V_1 - V_p = V_2 - V_p$ corresponds to an eigenenergy difference of the $J_{\text{eff}} = 1/2$ doublet and the p orbitals when no electron occupies them.

C. Building Kitaev-Heisenberg model

We can build the Kitaev-Heisenberg model

$$\mathcal{H}_{\text{KH}} = \sum_{a=x,y,z} \sum_{\langle i,j \rangle_a} (K S_i^a S_j^a + J_H \mathbf{S}_i \cdot \mathbf{S}_j) - \sum_j \mathbf{h} \cdot \mathbf{S}_j, \quad (\text{S1.21})$$

on the honeycomb lattice from the spin Hamiltonian (3) in the main text. Note that we put two triangles $\triangle M_1-L_1-M_2$ and $\triangle M_1-L_1-M_2$ on the xy plane to derive the Hamiltonian (3) of the main text. The M_1-M_2 bond in this spin Hamiltonian corresponds to the zz bond (the red line) of Fig. S2 (a). The other bonds $a = x, y$ are derived similarly. Let us consider the xx bond of Fig. S2 (b). We consider a local $x'y'z'$ coordinate system and put triangles $\triangle M_3-L_3-M_4$ and $\triangle M_3-L_4-M_4$ on the $x'y'$ plane and derive the effective spin Hamiltonian,

$$\mathcal{H}_{\text{spin}} = P \left[K S_3^{z'} S_4^{z'} + J_F \mathbf{S}_3 \cdot \mathbf{S}_4 - \sum_{j=3,4} \mathbf{h} \cdot \mathbf{S}_j \right] P. \quad (\text{S1.22})$$

To combine the octahedra of Figs. S2 (a) and (b) so as to make them share an edge and form the green M_2-M_3 bond, the xyz and $x'y'z'$ coordinates should satisfy

$$(x', y', z') = (y, z, x), \quad (\text{S1.23})$$

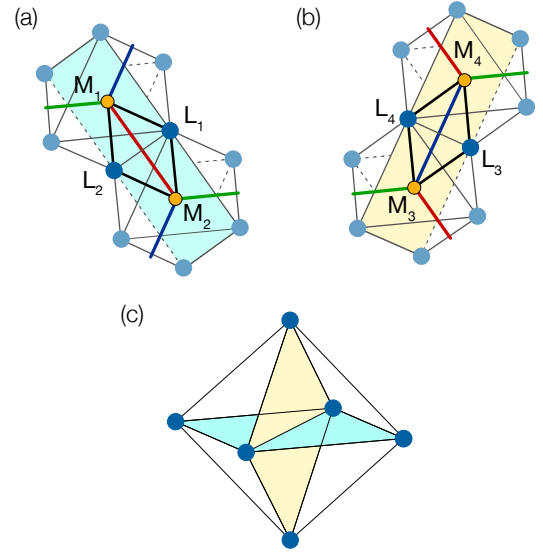


FIG. S2. (a) zz bond (red line) of Kitaev-Heisenberg model on xy plane (light blue plane). (b) xx bond (blue line) of Kitaev-Heisenberg model on yz plane (light yellow plane). (c) Orthogonality of two planes.

turning Eq. (S1.22) into

$$\mathcal{H}_{\text{spin}} = P \left[K S_3^x S_4^x + J_F \mathbf{S}_3 \cdot \mathbf{S}_4 - \sum_{j=3,4} \mathbf{h} \cdot \mathbf{S}_j \right] P. \quad (\text{S1.24})$$

In fact, we can easily confirm the relation (S1.23) by overlapping the xy and $x'y'$ planes with a single octahedron [Fig. S2 (c)]. Repeating the same procedure, we obtain the Kitaev-Heisenberg model (S1.21) on the honeycomb lattice.

D. In-plane electric fields

Now, we apply the in-plane electric field $\mathbf{E} = E^x \mathbf{e}_x + E^y \mathbf{e}_y$ to the $J_{\text{eff}} = 1/2$ model. Recall that we put the three-site model on the xy plane. The in-plane electric field breaks the C_2 rotation symmetry and the σ_v reflection symmetry about the $y = x$ plane. The remaining symmetry is the σ'_v reflection symmetry about the xy plane. The in-plane electric field permits hoppings that were intrinsically forbidden. The in-plane DC electric field induces hoppings between p orbitals and t_{2g} orbitals,

$$\begin{aligned} \delta\mathcal{H}_t(\mathbf{E}) = & -I \sum_{\sigma=\pm} [E^y (p_{z,\sigma}^\dagger d_{1,yz,\sigma} + p_{x,\sigma}^\dagger d_{1,xy,\sigma}) \\ & + E^x (p_{z,\sigma}^\dagger d_{2,yz,\sigma} + p_{y,\sigma}^\dagger d_{2,xy,\sigma}) + \text{H.c.}], \end{aligned} \quad (\text{S1.25})$$

where $-IE^y$ is the matrix element of the $-E^y P^y$ term in the single-electron Hamiltonian:

$$\begin{aligned} -IE^y &= \langle p_{x,\sigma} | (-E^y P^y) | d_{1,xy,\sigma} \rangle \\ &= -eE^y \int d\mathbf{r} \langle p_{x,\sigma} | \mathbf{r} \rangle y \langle \mathbf{r} | d_{j,xy,\sigma} \rangle. \end{aligned} \quad (\text{S1.26})$$

To evaluate the constant I , we adopt the wave functions $\langle \mathbf{r} | d_{j,xy,\sigma} \rangle$ and $\langle \mathbf{r} | p_{xy,\sigma} \rangle$ of the hydrogen-like atom in terms of the the polar coordinate $\mathbf{r} = r(\sin\theta \cos\phi, \sin\theta \sin\phi, \cos\theta)$:

$$\langle \mathbf{r} | d_{j,xy,\sigma} \rangle \approx R_{nd}(r) Y_{xy}(\theta, \phi), \quad (\text{S1.27})$$

$$\langle \mathbf{r} | p_{x,\sigma} \rangle \approx R_{2p}(r) Y_x(\theta, \phi), \quad (\text{S1.28})$$

$$R_{3d}(r) = \frac{4}{81\sqrt{30}} \left(\frac{Z_M}{a_0}\right)^{3/2} \left(\frac{Z_M r}{a_0}\right)^2 \exp\left(-\frac{Z_M r}{3a_0}\right), \quad (\text{S1.29})$$

$$\begin{aligned} R_{4d}(r) &= \frac{1}{768\sqrt{5}} \left(\frac{Z_M}{a_0}\right)^{3/2} \left(12 - \frac{Z_M r}{a_0}\right) \left(\frac{Z_M r}{a_0}\right)^2 \\ &\times \exp\left(-\frac{Z_M r}{4a_0}\right), \end{aligned} \quad (\text{S1.30})$$

$$R_{2p}(r) = \frac{1}{2\sqrt{6}} \left(\frac{Z_L}{a_0}\right)^{3/2} \frac{Z_L}{a_0} r \exp\left(-\frac{Z_L}{2a_0} r\right), \quad (\text{S1.31})$$

$$Y_{xy}(\theta, \phi) = \sqrt{\frac{15}{16\pi}} \sin^2\theta \sin(2\phi), \quad (\text{S1.32})$$

$$Y_x(\theta, \phi) = \sqrt{\frac{3}{4\pi}} \sin\theta \cos\phi. \quad (\text{S1.33})$$

Here, a_0 , Z_M , and Z_L are the Bohr radius and the atomic numbers of M_j and L , respectively [46, 64]. $n = 3, 4, \dots$ represent the principal quantum number. For $n = 3$, these wave functions lead to

$$I \approx ea_0 \frac{16}{27} Z_M^{7/2} Z_L^{5/2} \left(\frac{Z_M}{3} + \frac{Z_L}{2}\right)^{-7}. \quad (\text{S1.34})$$

For $n = 4$, it becomes

$$I \approx ea_0 \frac{\sqrt{3}}{16} Z_M^{7/2} Z_L^{5/2} \left(\frac{Z_M}{4} + \frac{Z_L}{2}\right)^{-8}. \quad (\text{S1.35})$$

Note the following symmetry,

$$\langle p_{a,\sigma} | P^b | d_{1,ab,\sigma} \rangle = I, \quad (\text{S1.36})$$

for $a, b = x, y, z$ and $a \neq b$. In analogy with the intrinsic hoppings $\mathcal{H}_t(\mathbf{0})$, we replace the t_{2g} -orbital operators with the Γ_{7+} ones:

$$\begin{aligned} \delta\mathcal{H}_t(\mathbf{E}) \sim & -\frac{I}{\sqrt{3}} \sum_{\sigma=\pm} [E^y (\sigma p_{z,-\sigma}^\dagger + p_{x,\sigma}^\dagger) d_{1,\Gamma_{7+},\sigma} \\ & + E^x (\sigma p_{z,-\sigma}^\dagger + p_{y,\sigma}^\dagger) d_{2,\Gamma_{7+},\sigma} \\ & + \text{H.c.}], \end{aligned} \quad (\text{S1.37})$$

where \sim denotes the approximate identity relation at low energies. The \mathbf{E} -induced hopping adds the following interactions to the spin Hamiltonian $\mathcal{H}_{\text{spin}}$:

$$\begin{aligned} P\delta\mathcal{H}_t(\mathbf{E}) & \left(\frac{1}{E_g - \mathcal{H}_U} Q\mathcal{H}_t(\mathbf{0})\right)^3 P + P\mathcal{H}_t(\mathbf{0}) \frac{1}{E_g - \mathcal{H}_U} Q\delta\mathcal{H}_t(\mathbf{E}) \left(\frac{1}{E_g - \mathcal{H}_U} Q\mathcal{H}_t(\mathbf{0})\right)^2 P \\ & + P\mathcal{H}_t(\mathbf{0}) \frac{1}{E_g - \mathcal{H}_U} Q\mathcal{H}_t(\mathbf{0}) \frac{1}{E_g - \mathcal{H}_U} Q\delta\mathcal{H}_t(\mathbf{E}) \frac{1}{E_g - \mathcal{H}_U} Q\mathcal{H}_t(\mathbf{0}) P \\ & + P\mathcal{H}_t(\mathbf{0}) \left(\frac{1}{E_g - \mathcal{H}_U} Q\mathcal{H}_t(\mathbf{0})\right)^2 \frac{1}{E_g - \mathcal{H}_U} Q\delta\mathcal{H}_t(\mathbf{E}) P \end{aligned} \quad (\text{S1.38})$$

Equation (S1.38) denotes the $O(|\mathbf{E}|^1)$ terms of diagrams in Fig. 2. Straightforward calculations for a triangle ΔM_1-L-M_2 lead to

$$\mathcal{H}_{\text{spin}} = J_{\text{F}} \mathbf{S}_1 \cdot \mathbf{S}_2 + K S_1^z S_2^z + \mathbf{D}_{\text{F}} \cdot \mathbf{S}_1 \times \mathbf{S}_2, \quad (\text{S1.39})$$

with $\mathbf{D}_{\text{F}} = D_{\text{F}}^z \mathbf{e}_z$ and

$$\frac{D_{\text{F}}^z}{J_{\text{F}}} = -\frac{4I}{t} \frac{(E^x + E^y)(U_d - U_p + \Delta_{dp}) + (E^x - E^y)J_{\text{H}}}{2(U_d - U_p) + J_{\text{H}}}. \quad (\text{S1.40})$$

E. Out-of-plane electric field

In contrast to the in-plane electric field, the out-of-plane electric field $\mathbf{E} = E^y \mathbf{e}_z$ keeps the σ_v reflection symmetry about the $y = x$ plane but breaks the σ'_v one about the $z = 0$ plane. It induces hoppings,

$$\begin{aligned} \delta\mathcal{H}_t(\mathbf{E}) &= -IE^z \sum_{\sigma=\pm} \sum_{j=1,2} [(p_{y,\sigma}^\dagger + p_{x,\sigma}^\dagger)d_{1,yz,\sigma} + \text{H.c.}] \\ &\sim -\frac{IE^z}{\sqrt{3}} \sum_{\sigma,j} [(\sigma p_{y,-\sigma}^\dagger + i p_{x,-\sigma}^\dagger)d_{j,\Gamma_{\tau+},\sigma} + \text{H.c.}], \end{aligned} \quad (\text{S1.41})$$

leading to

$$\begin{aligned} \mathcal{H}_{\text{spin}} &= J_{\text{F}} \mathbf{S}_1 \cdot \mathbf{S}_2 + K S_1^z S_2^z + \mathbf{D}_{\text{F}} \cdot \mathbf{S}_1 \times \mathbf{S}_2 \\ &\quad + \Gamma' [(S_1^x + S_1^y) S_2^z + S_1^z (S_2^x + S_2^y)] \end{aligned} \quad (\text{S1.42})$$

with

$$\begin{aligned} \mathbf{D}_{\text{F}} &= D_{\text{F}}^x (\mathbf{e}_x + \mathbf{e}_y), \quad (\text{S1.43}) \\ D_{\text{F}}^x &= \frac{16}{3} E^z I \left(\frac{1}{U_d - U_p + \Delta_{dp}} \right)^2 \\ &\quad \cdot \frac{J_{\text{H}}}{4(U_d - U_p + \Delta_{dp})^2 - J_{\text{H}}^2}, \end{aligned} \quad (\text{S1.44})$$

$$\begin{aligned} \Gamma' &= \frac{32t^3}{9} E^z I \left(\frac{1}{U_d - U_p + \Delta_{dp}} \right)^2 \\ &\quad \cdot \frac{U_d - U_p + \Delta_{dp}}{4(U_d - U_p + \Delta_{dp})^2 - J_{\text{H}}^2}. \end{aligned} \quad (\text{S1.45})$$

F. Kitaev-Heisenberg- Γ' model under [111] electric field

When we build the Kitaev honeycomb model from our three-site models [Figs. S2 (a) and (b)], the honeycomb lattice is put on the (111) plane. Now we apply the electric field $\mathbf{E}_{[111]} = E_{[111]}(\mathbf{e}_x + \mathbf{e}_y + \mathbf{e})/\sqrt{3}$ so that the electric field is perpendicular to the honeycomb lattice. Then, the resultant spin Hamiltonian is given by

$$\begin{aligned} \mathcal{H}_{\text{KH}\Gamma'} &= \sum_{a=x,y,z} \sum_{\langle i,j \rangle_a} (K S_i^a S_j^a + J_{\text{H}} \mathbf{S}_i \cdot \mathbf{S}_j) - \sum_j \mathbf{h} \cdot \mathbf{S}_j \\ &\quad + \Gamma'(\mathbf{E}_{[111]}) \sum_{a=x,y,z} \sum_{b,c \neq a} \sum_{\langle i,j \rangle_a} (S_i^b S_j^c + S_i^c S_j^b), \end{aligned} \quad (\text{S1.46})$$

where $\Gamma'(\mathbf{E}_{[111]})$ is proportional to $E_{[111]}$:

$$\begin{aligned} \Gamma' &= \frac{32t^3}{9} \frac{2E_{[111]}}{\sqrt{3}} I \left(\frac{1}{U_d - U_p + \Delta_{dp}} \right)^2 \\ &\quad \cdot \frac{U_d - U_p + \Delta_{dp}}{4(U_d - U_p + \Delta_{dp})^2 - J_{\text{H}}^2}. \end{aligned} \quad (\text{S1.47})$$

We assumed that the ligand sites are all crystallographically equivalent, where the DMI is canceled in the many-body Hamiltonian (S1.46).

S2. RASHBA SPIN-ORBIT INTERACTION IN TIGHT-BINDING MODELS

Here, we remove the intra-atomic SOC but add the inter-atomic SOC, the Rashba SOC. The Rashba SOC enters into the single-electron Hamiltonian \hat{H}_1 :

$$\hat{H}_1 = \frac{\mathbf{p}^2}{2m} + V(\mathbf{r}) - \alpha_{\text{R}} \mathbf{e}(\mathbf{r}) \cdot \boldsymbol{\sigma} \times \mathbf{p}, \quad (\text{S2.48})$$

where \mathbf{p} and m are the momentum and the mass of the electron and $V(\mathbf{r})$ is the potential that the electron feels. $\mathbf{e}(\mathbf{r}) = \mathbf{E}(\mathbf{r})/|\mathbf{E}(\mathbf{r})|$ is the unit vector parallel to the electric field as defined in the main text. We normalized $\mathbf{e}(\mathbf{r})$ to make $\alpha_{\text{R}} \propto |\mathbf{E}(\mathbf{r})|$ following the convention. The single-electron Hamiltonian keeps the C_{2v} symmetry [64] in the absence of the electric and magnetic fields (i.e., $\mathbf{E}(\mathbf{r}) = \mathbf{h} = \mathbf{0}$). The last term of \hat{H}_1 is nothing but the Rashba SOC. The Rashba SOC enters into the second-quantized many-electron model via the hopping amplitude, a matrix element of the single-electron Hamiltonian. The hopping amplitude between the p_x orbital at L and the d_a orbital at M_j is given by

$$\langle p_{x,s} | \hat{H}_1 | d_{j,a,s'} \rangle. \quad (\text{S2.49})$$

When $\mathbf{E}(\mathbf{r}) = \mathbf{0}$, the hopping amplitude in our three-site model on the isosceles right triangle is reduced to

$$\langle p_{x,s} | \hat{H}_1 | d_{j,a,s'} \rangle = t \delta_{a,xy} \delta_{j,2} \delta_{s,s'}, \quad (\text{S2.50})$$

with a real constant t [see Fig. S1 (d)]. The Rashba SOC adds another term to the right hand side of Eq. (S2.50). For example, $\mathbf{E}(\mathbf{r}) = E^z \mathbf{e}_z$ gives

$$\begin{aligned} &\langle p_{x,s} | (-\alpha_{\text{R}} \mathbf{e}(\mathbf{r}) \cdot \boldsymbol{\sigma} \times \mathbf{p}) | d_{j,a,s'} \rangle \\ &= -\alpha_{\text{R}} |\mathbf{k}| e^z (\boldsymbol{\sigma}^{ss'} \times (-i\mathbf{d}_j))^z \delta_{j,2}, \end{aligned} \quad (\text{S2.51})$$

where we replaced the momentum $\mathbf{p} = \hbar\mathbf{k}$ by $-i\hbar|\mathbf{k}|\mathbf{d}_j$ with the unit vector \mathbf{d}_j parallel to the M_j -L bond. The Kronecker's delta $\delta_{j,2}$ appears because the vector \mathbf{d}_j is proportional to \mathbf{e}_x for $j = 1$ and to \mathbf{e}_y for $j = 2$. Hence, we arrived at the \mathbf{E} -induced hoppings (5) in the main text.

S3. STRENGTH OF EXTERNAL AND INTERNAL ELECTRIC FIELDS

This section gives brief supplemental information to the estimation of required electric-field strength. Mainly, there are two resources of the DC electric field. One is to apply it externally using, for example, field-effect transistors. The other is generated internally by crystal structures. We call the former external electric fields and the latter internal ones.

Currently, we can realize the external DC field of the strength ~ 10 MV/cm using, for example, double-layer transistors [52, 53]. On the other hand, the internal DC

electric field can be even stronger. Let us consider the octahedral CEF [See Figs. S2 (a), (b), and S3]. The strength of the CEF is typically ~ 1 eV [80]. If the ligand is ~ 0.1 – 1 nm away from the magnetic ion, the internal CEF is ~ 10 – 100 MV/cm. This internal CEF is responsible for the Rashba SOC generated on the interface of different materials. This is the reason why the Rashba SOC can be strong, as we briefly saw in the main text. We can find another interesting situation in scanning tunneling microscopes (STM). A tip of the STM induces a DC electric field strong enough to induce the tunneling electron current on the surface. If the STM tip is ~ 1 nm distant from the surface and the ~ 1 V voltage is applied, the surface feels the ~ 10 MV/cm electric field [57].

S4. FIELD-INDUCED DZYALOSHINSKII-MORIYA INTERACTION IN MINIMAL MODEL

The main text discusses the intra-atomic SOC in the d orbital and the inter-atomic SOC. By contrast, this section discusses a simple model with a weak intra-atomic SOC within the ligand site to supplement the main text. Also, we suppose a d^9 electron configuration unlike the models discussed in the main text. Let us name this model a minimal model after its simplicity.

A. Hybridization of p orbitals

To define the minimal model Hamiltonian, we briefly review the hybridization of p orbitals. Let us denote the eigenenergy of the s and p orbitals in the absence of SOC as ε_s and ε_p , respectively. The Hamiltonian to describe the hybridization is given by

$$\mathcal{H}_{sp} = \sum_{n=1}^8 c_n^\dagger H_{sp} c_n, \quad (\text{S4.52})$$

where c_n^\dagger denotes the creation operators of the s -orbital electron (s_\pm^\dagger) and the p -orbital ones ($p_{\mu,\pm}^\dagger$ for $\mu = x, y, z$). We list them as follows.

$$\begin{aligned} & (c_1^\dagger, c_2^\dagger, \dots, c_8^\dagger) \\ & = (s_+^\dagger, p_{x,+}^\dagger, p_{y,+}^\dagger, p_{z,-}^\dagger, s_-^\dagger, p_{x,-}^\dagger, p_{y,-}^\dagger, p_{z,+}^\dagger). \end{aligned} \quad (\text{S4.53})$$

Note that the spin of the p_z orbitals in Eq. (S4.53) are inverted in advance to simplify H_{sp} . H_{sp} contains the eigenenergies, ε_s and ε_p , of the s and p orbitals, the uniaxial anisotropy Δ , and SOC $\lambda \mathbf{L}_p \cdot \mathbf{S}_p$, where the eigenenergies ε_s and ε_p are supposed to be those in the absence of the anisotropy or SOC. The 8×8 matrix H_{sp} is then

block-diagonalized.

$$\begin{aligned} H_{sp} &= \begin{pmatrix} \varepsilon_s & 0 & 0 & 0 & 0 & 0 & 0 & 0 \\ 0 & \varepsilon_p & -i\frac{\lambda}{2} & \frac{\lambda}{2} & 0 & 0 & 0 & 0 \\ 0 & i\frac{\lambda}{2} & \varepsilon_p & -i\frac{\lambda}{2} & 0 & 0 & 0 & 0 \\ 0 & \frac{\lambda}{2} & i\frac{\lambda}{2} & \varepsilon_p + \Delta & 0 & 0 & 0 & 0 \\ 0 & 0 & 0 & 0 & \varepsilon_s & 0 & 0 & 0 \\ 0 & 0 & 0 & 0 & 0 & \varepsilon_p & i\frac{\lambda}{2} & -\frac{\lambda}{2} \\ 0 & 0 & 0 & 0 & 0 & -i\frac{\lambda}{2} & \varepsilon_p & -i\frac{\lambda}{2} \\ 0 & 0 & 0 & 0 & 0 & -\frac{\lambda}{2} & i\frac{\lambda}{2} & \varepsilon_p + \Delta \end{pmatrix} \\ &= \begin{pmatrix} \varepsilon_s & 0 & 0 & 0 \\ 0 & H_{p-} & 0 & 0 \\ 0 & 0 & \varepsilon_s & 0 \\ 0 & 0 & 0 & H_{p+} \end{pmatrix}. \end{aligned} \quad (\text{S4.54})$$

Here, we did not include the sp hybridization for simplicity though it is straightforward to include the sp hybridization as evident from the matrix representation (S4.54). Ignoring the s orbital is consistent with an approximation performed later in this Section.

The 3×3 matrix $H_{p\pm}$ describes the hybridization of $|p_{x,\mp}\rangle$, $|p_{y,\mp}\rangle$, and $|p_{z,\pm}\rangle$.

$$H_{p+} = \begin{pmatrix} \varepsilon_p & i\frac{\lambda}{2} & -\frac{\lambda}{2} \\ -i\frac{\lambda}{2} & \varepsilon_p & -i\frac{\lambda}{2} \\ -\frac{\lambda}{2} & i\frac{\lambda}{2} & \varepsilon_p + \Delta \end{pmatrix}. \quad (\text{S4.55})$$

H_{p-} is obtained from H_{p+} by replacing $\lambda \rightarrow -\lambda$ and $i \rightarrow -i$. Performing the first-order perturbation with respect to λ , we obtain the hybridization of p orbitals.

$$|\tilde{p}_{z,+}\rangle = |p_{z,+}\rangle - \frac{\lambda}{2\Delta} (|p_{x,-}\rangle + i|p_{y,-}\rangle), \quad (\text{S4.56})$$

$$|\tilde{p}_{x,-}\rangle + i|\tilde{p}_{y,-}\rangle = |p_{x,-}\rangle + i|p_{y,-}\rangle + \frac{\lambda}{\Delta} |p_{z,+}\rangle, \quad (\text{S4.57})$$

$$|\tilde{p}_{x,-}\rangle - i|\tilde{p}_{y,-}\rangle = |p_{x,-}\rangle - i|p_{y,-}\rangle, \quad (\text{S4.58})$$

where $|\tilde{p}_{\mu,\sigma}\rangle =: \tilde{p}_{\mu,\sigma}^\dagger |0\rangle$ denotes the hybridized p_μ -orbital state. The hybridizations of $|p_{x,+}\rangle$, $|p_{y,+}\rangle$, and $|p_{z,-}\rangle$ are derived likewise.

$$|\tilde{p}_{z,-}\rangle = |p_{z,-}\rangle + \frac{\lambda}{2\Delta} (|p_{x,+}\rangle - i|p_{y,-}\rangle), \quad (\text{S4.59})$$

$$|\tilde{p}_{x,+}\rangle - i|\tilde{p}_{y,+}\rangle = |p_{x,+}\rangle - i|p_{y,+}\rangle - \frac{\lambda}{\Delta} |p_{z,+}\rangle, \quad (\text{S4.60})$$

$$|\tilde{p}_{x,+}\rangle + i|\tilde{p}_{y,+}\rangle = |p_{x,+}\rangle + i|p_{y,+}\rangle. \quad (\text{S4.61})$$

B. Model

The minimal model has the following electron many-body Hamiltonian.

$$\mathcal{H} = \mathcal{H}_U + \mathcal{H}_t(\mathbf{0}) + \delta\mathcal{H}_t(\mathbf{E}), \quad (\text{S4.62})$$

$$\mathcal{H}_U = U_d \sum_{j=1,2} n_{j,a_{1g},+} + n_{j,a_{1g},-} + U_p n_{p_z,+} + n_{p_z,-}$$

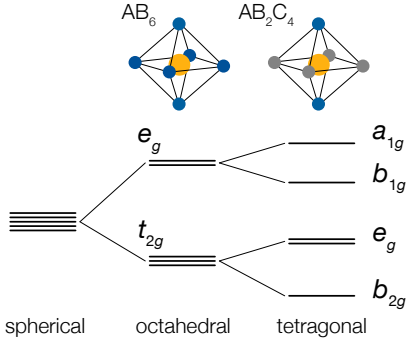


FIG. S3. Splittings of d orbitals by octahedral and tetragonal CEF [64]. The tetragonal CEF derives from the octahedral one in the AB_6 unit of a crystal by replacing four of B atoms with C atoms or distorting AB_6 uniaxially.

$$+ \sum_{j=1,2} V_j \sum_{\sigma=\pm} n_{j,a_{1g},\sigma} + V_p \sum_{\sigma=\pm} n_{p_{z,\sigma}}, \quad (\text{S4.63})$$

$$\mathcal{H}_t(\mathbf{0}) = t \sum_{j=1,2} \sum_{\sigma=\pm} (-1)^j (p_{z,\sigma}^\dagger d_{j,a_{1g},\sigma} + \text{H.c.}), \quad (\text{S4.64})$$

$$\delta\mathcal{H}_t(\mathbf{E}) = -I \sum_{j=1,2} \sum_{\sigma=\pm} [(E^x p_{x,\sigma}^\dagger + E^y p_{y,\sigma}^\dagger) d_{j,a_{1g},\sigma} + \text{H.c.}], \quad (\text{S4.65})$$

where $n_{j,a_{1g},\sigma} := d_{j,a_{1g},\sigma}^\dagger d_{j,a_{1g},\sigma}$ and $n_{p_{z,\sigma}} = p_{z,\sigma}^\dagger p_{z,\sigma}$ number operator of the a_{1g} -orbital electron at M_j and the non-hybridized p_z orbital at the ligand site, respectively. The eigenenergies of the a_{1g} orbital and the p_z orbital are encoded in the on-site potentials V_j and V_p [58, 59]. U_d and U_p represent the on-site Coulomb interaction. Generally, DC electric fields also affect the intra-atomic interaction (S4.63), as we mentioned in the main text. However, we do not consider it for the following reason. The extrinsic hopping amplitude in Eq. (S4.65) is proportional to E^a . Hence, as long as we are focused on additional spin-spin interactions generated by \mathbf{E} with the $O(|\mathbf{E}|^1)$ precision, we can keep $\mathcal{H}_U(\mathbf{E}) \approx \mathcal{H}_U(\mathbf{0})$.

We consider the d^9 configuration at M_j and regard the a_{1g} orbital among them is half filled (Fig. S3). In other words, we assume a tetragonal CEF at each M_j . The tetrahedral CEF lifts the d -orbital degeneracy. Note that an octahedral CEF is a special case of the tetragonal one. The octahedral CEF lifts the d orbitals into e_g and t_{2g} . The tetragonal CEF with the lower symmetry than the octahedral one further splits e_g into a_{1g} and b_{1g} and t_{2g} into e_g and b_{2g} [64]. The a_{1g} orbital has the $d_{3z^2-r^2}$ symmetry and thus the highest eigenenergy under the tetragonal CEF.

We incorporate the DC electric field into the extrinsic hoppings (S4.65). The Hamiltonian (S4.62) does not include the p -orbital hybridization. It is straightforward to take it into account. Recall that all the p -orbital levels are below the Fermi surface and the p_z one is closest

to the Fermi surface. At low energies, we keep the hybridized p_z orbital only. Hence, we simply replace $p_{z,\pm}$ in Eqs. (S4.63) and (S4.64) with $\tilde{p}_{z,\pm}$. On the other hand, the extrinsic hoppings (S4.65) are involved with the operators $p_{x,\sigma}$ and $p_{y,\sigma}$ other than the low-energy relevant orbital. Since it costs too large energy to excite \tilde{p}_x - and \tilde{p}_y -orbital states, the term (S4.65) would seem irrelevant to low-energy physics. However, this is not the case because $\tilde{p}_{x,\sigma}$ and $\tilde{p}_{y,\sigma}$ can remove an electron from the \tilde{p}_z orbital with a small probability. The probability is given by $(\lambda/2\Delta)^2$ according to Eqs. (S4.56) and (S4.59). Eqs. (S4.56) and (S4.59) gives

$$P p_{x,\sigma}^\dagger P = 0, \quad Q p_{x,\sigma}^\dagger P = Q \left(\sigma \frac{\lambda}{2\Delta} \tilde{p}_{z,-\sigma}^\dagger \right) P, \quad (\text{S4.66})$$

$$P p_{y,\sigma}^\dagger P = 0, \quad Q p_{y,\sigma}^\dagger P = Q \left(-i \frac{\lambda}{2\Delta} \tilde{p}_{z,-\sigma}^\dagger \right) P, \quad (\text{S4.67})$$

because the projection operator P acts on the ligand site as $P = |\tilde{p}_{z,+}\rangle \langle \tilde{p}_{z,+}| + |\tilde{p}_{z,-}\rangle \langle \tilde{p}_{z,-}|$. Therefore, we may approximate

$$p_{x,\sigma}^\dagger \approx \sigma \frac{\lambda}{2\Delta} \tilde{p}_{z,-\sigma}^\dagger, \quad p_{y,\sigma}^\dagger \approx -i \frac{\lambda}{2\Delta} \tilde{p}_{z,-\sigma}^\dagger, \quad (\text{S4.68})$$

at low energies and rewrite the extrinsic hoppings (S4.65) as

$$\delta\mathcal{H}_t(\mathbf{E}) \approx \frac{I\lambda}{2\Delta} \sum_{j=1,2} \sum_{\sigma=\pm} [(E^x \sigma \tilde{p}_{z,-\sigma}^\dagger + i E^y \tilde{p}_{z,-\sigma}^\dagger) d_{j,a_{1g},\sigma} + \text{H.c.}], \quad (\text{S4.69})$$

at low temperatures. Hereafter, we drop the tilde in the creation and annihilation operators (i.e., $\tilde{p}_{z,\sigma} \rightarrow p_{z,\sigma}$) to simplify the notation.

C. Symmetries

When $\mathbf{E} = \mathbf{0}$, the minimal model has the D_{4h} symmetry due to the tetragonal CEF at the M_j sites. The linear M_1 -L- M_2 alignment as well as the uniaxial CEF at the ligand site respect the D_{4h} symmetry. The D_{4h} group contains D_{2h} as its subgroup made of C_{2a} rotations ($a = x, y, z$), σ_a reflections ($a = xy, yz, zx$), and an inversion at the ligand site. The D_{2h} symmetry is evident from the geometrical structure of the model such as the equidistant linear alignment of the three sites and the tetragonal CEF.

SOC, $\lambda \mathbf{l}_p \cdot \mathbf{s}_p$, transcribes the D_{4h} crystalline symmetry into a spin symmetry, where \mathbf{l}_p and \mathbf{s}_p are the orbital angular momentum and the spin due to the p orbitals, respectively. The spin operator \mathbf{s}_p is defined as

$$\mathbf{s}_p := \frac{1}{2} \sum_{\mu=x,y,z} \sum_{s,s'=\pm} p_{\mu,s}^\dagger \boldsymbol{\sigma}^{ss'} p_{\mu,s'}, \quad (\text{S4.70})$$

where $\boldsymbol{\sigma} = (\sigma^x, \sigma^y, \sigma^z)$ represents the Pauli matrices and $\boldsymbol{\sigma}^{ss'}$ denotes their (s, s') components. If SOC was absent,

the minimal model has the $D_{4h} \times \text{SU}(2)$ symmetry, a direct product of the D_{4h} crystalline symmetry and the $\text{SU}(2)$ spin-rotation symmetry. SOC violates the $\text{SU}(2)$ symmetry down to D_{4h} in the following sense. For example, SOC is antisymmetric under the inversion $\mathbf{r} \rightarrow -\mathbf{r}$ because it turns $(\mathbf{l}_p, \mathbf{s}_p) \rightarrow (-\mathbf{l}_p, \mathbf{s}_p)$, but symmetry under the simultaneous inversion $(\mathbf{l}_p, \mathbf{s}_p) \rightarrow (-\mathbf{l}_p, -\mathbf{s}_p)$ of the real space and the spin space. SOC lowers the symmetry $D_{4h} \times \text{SU}(2) \rightarrow D_{4h}$. We denote the latter D_{4h} as \tilde{D}_{4h} to distinguish it from the pure crystalline symmetry. An arbitrary element $M \in \tilde{D}_{4h}$ acts on \mathbf{l}_p and \mathbf{s}_p equivalently. In other words, M treats \mathbf{s}_p as if it was an angular momentum. Then, the following invariance is obvious.

$$M(\lambda \mathbf{l}_p \cdot \mathbf{s}_p)M^{-1} = \lambda \mathbf{l}_p \cdot \mathbf{s}_p. \quad (\text{S4.71})$$

We can translate the \tilde{D}_{4h} -group operation in terms of $p_{\mu,\sigma}^\dagger$ operators. For example, the C_{2z} rotation of \tilde{D}_{4h} turns them into

$$C_{2z}(p_{x,\sigma}^\dagger, p_{y,\sigma}^\dagger, p_{z,\sigma}^\dagger)C_{2z}^{-1} = i\sigma(-p_{x,\sigma}^\dagger, -p_{y,\sigma}^\dagger, p_{z,\sigma}^\dagger). \quad (\text{S4.72})$$

Operations of the \tilde{D}_{4h} group on $p_{\mu,\sigma}^\dagger$ are defined likewise. Hence, we find \tilde{D}_{4h} keeps the whole intra-atomic interactions at the ligand site invariant.

The \tilde{D}_{4h} symmetry acts on \mathbf{S}_j carried by the a_{1g} orbital similarly to \mathbf{s}_p . To represent it in terms of $d_{j,a_{1g},\sigma}^\dagger$, we need to reflect the a_{1g} spatial symmetry. For example, C_{2z} acts $d_{j,a_{1g},\sigma}^\dagger$ as

$$C_{2z}d_{j,a_{1g},\sigma}^\dagger C_{2z}^{-1} = i\sigma d_{j,a_{1g},\sigma}. \quad (\text{S4.73})$$

In terms of the spin $\mathbf{S}_j := \frac{1}{2} \sum_{s,s'} d_{j,a_{1g},s}^\dagger \boldsymbol{\sigma}^{ss'} d_{j,a_{1g},s'}$, the relation (S4.73) can read as

$$C_{2z}\mathbf{S}_j C_{2z}^{-1} = (-S_j^x, -S_j^y, S_j^z)^\top, \quad (\text{S4.74})$$

where \top denotes the transpose. The transformation (S4.74) accords with the aforementioned requirement that \mathbf{S}_j transforms similarly to the orbital angular momentum \mathbf{l}_p .

Now we can confirm that the full Hamiltonian (S4.62) satisfies $C_{2z}\mathcal{H}C_{2z}^{-1} = \mathcal{H}$. We can see that D_{4h} -noninvariant hoppings such as $p_{y,\sigma}^\dagger d_{j,a_{1g},\sigma}$ are absent in the minimal model because of $C_{2z}p_{y,\sigma}^\dagger d_{j,a_{1g},\sigma} C_{2z}^{-1} = -p_{y,\sigma}^\dagger d_{j,a_{1g},\sigma}$. Similar arguments hold for the other members of the \tilde{D}_{4h} group.

D. Without electric fields

Note that both the CEF at M_j and the ligand site respect the D_{4h} symmetry other than the inversion. The inversion symmetry exists because the ligand site is precisely located at the inversion center of the M_1 - M_2 bond.

Indeed, the resultant spin Hamiltonian fully respects the \tilde{D}_{4h} symmetry. In particular, the spin Hamiltonian cannot have the DMI owing to the inversion symmetry. The spin Hamiltonian $\mathcal{H}_{\text{spin}}$ is given by Eq. (1) of the main text. When $\mathbf{E} = \mathbf{0}$, all the \mathcal{H}_t in Eq. (1) are supposed to be $\mathcal{H}_t(\mathbf{0})$:

$$\mathcal{H}_{\text{spin}} = P\mathcal{H}_t(\mathbf{0})\left(\frac{1}{E_g - \mathcal{H}_U}Q\mathcal{H}_t(\mathbf{0})\right)^3 P, \quad (\text{S4.75})$$

in the absence of the magnetic field. Carrying out the fourth-order expansion, we find

$$\begin{aligned} \mathcal{H}_{\text{spin}} &= J_{\text{min}}\mathbf{S}_1 \cdot \mathbf{S}_2, \quad (\text{S4.76}) \\ J_{\text{min}} &= 4t^4 \frac{1}{(U_d - U_p + \Delta_{dp})^2} \left(\frac{2}{2\Delta_{dp} + U_d - U_p} + \frac{1}{U_d} \right), \quad (\text{S4.77}) \end{aligned}$$

where the parameters Δ_{dp} , U_d , U_p are defined similarly to the other models discussed in the main text.

E. With electric fields

The electric field adds the hopping (S4.69) into the perturbation expansion. Collecting all the $O(|\mathbf{E}|^1)$ terms in the expansion of Fig. 2 of the main text, we find that the DC electric field $\mathbf{E} = E^x \mathbf{e}_x + E^y \mathbf{e}_y$ modifies the spin Hamiltonian from Eq. (S4.76) to

$$\mathcal{H}_{\text{spin}} = J_{\text{min}}\mathbf{S}_1 \cdot \mathbf{S}_2 + \mathbf{D}_{\text{min}} \cdot \mathbf{S}_1 \times \mathbf{S}_2, \quad (\text{S4.78})$$

$$\mathbf{D}_{\text{min}} = \alpha_{\text{min}} \mathbf{n}, \quad (\text{S4.79})$$

$$\mathbf{n} = \frac{1}{|\mathbf{E}|} (E^y \mathbf{e}_x - E^x \mathbf{e}_y), \quad (\text{S4.80})$$

$$\alpha_{\text{min}} = \frac{8|\mathbf{E}|t^3\lambda}{2\Delta} \frac{1}{(\Delta_{dp} + U_d - U_p)^2} \frac{1}{2\Delta_{dp} + 2U_d - U_p}. \quad (\text{S4.81})$$

F. DMI and symmetries

The electric field on the xy plane lowers the symmetry of the minimal model from D_{2h} to $C_{2v} = \{\mathbb{I}, C_{2e}, \sigma_{xy}, \sigma_{ez}\}$, where \mathbb{I} , C_{2e} , and σ_{ez} denote the identity, the C_2 rotation around \mathbf{E} , and the reflection along \mathbf{n} (i.e., $\mathbf{n} \rightarrow -\mathbf{n}$), respectively. The spin Hamiltonian (S4.78) respects the C_{2v} symmetry. To see this, we look into C_{2v} operations to DMI. To discuss those point-group operations, we can assume $\mathbf{E} = E\mathbf{e}_x$ and $\mathbf{n} = -\mathbf{e}_y$ without loss of generality. The $C_{2e} = C_{2x}$ rotation, the σ_{xy} and $\sigma_{ez} = \sigma_{zx}$ reflections act on the spin operator \mathbf{S}_j as

$$C_{2x}\mathbf{S}_j C_{2x}^{-1} = (S_j^x, -S_j^y, -S_j^z)^\top, \quad (\text{S4.82})$$

$$\sigma_{xy}\mathbf{S}_j \sigma_{xy}^{-1} = (S_j^x, S_j^y, -S_j^z)^\top, \quad (\text{S4.83})$$

$$\sigma_{zx}\mathbf{S}_j \sigma_{zx}^{-1} = (S_j^x, -S_j^y, S_j^z)^\top, \quad (\text{S4.84})$$

with $j' = j + 1 \pmod{2}$. The C_{2x} symmetry (S4.82) imposes a constraint, $(\mathbf{D}_{\min})^x = 0$, and the σ_{xy} symmetry

(S4.83) imposes $(\mathbf{D}_{\min})^z = 0$. The σ_{zx} symmetry (S4.84) imposes both the constraints, $(\mathbf{D}_{\min})^x = (\mathbf{D}_{\min})^z = 0$.

-
- [1] C. L. Kane and E. J. Mele, Z_2 Topological Order and the Quantum Spin Hall Effect, *Phys. Rev. Lett.* **95**, 146802 (2005).
- [2] C. L. Kane and E. J. Mele, Quantum Spin Hall Effect in Graphene, *Phys. Rev. Lett.* **95**, 226801 (2005).
- [3] C. Nayak, S. H. Simon, A. Stern, M. Freedman, and S. Das Sarma, Non-Abelian anyons and topological quantum computation, *Rev. Mod. Phys.* **80**, 1083 (2008).
- [4] M. Z. Hasan and C. L. Kane, Colloquium: Topological insulators, *Rev. Mod. Phys.* **82**, 3045 (2010).
- [5] X.-L. Qi and S.-C. Zhang, Topological insulators and superconductors, *Rev. Mod. Phys.* **83**, 1057 (2011).
- [6] Y. Ando, Topological Insulator Materials, *Journal of the Physical Society of Japan* **82**, 102001 (2013).
- [7] N. Nagaosa and Y. Tokura, Topological properties and dynamics of magnetic skyrmions, *Nature Nanotechnology* **8**, 899 (2013).
- [8] Y. Fujishiro, N. Kanazawa, and Y. Tokura, Engineering skyrmions and emergent monopoles in topological spin crystals, *Applied Physics Letters* **116**, 090501 (2020).
- [9] S. Trebst, Kitaev Materials, *arXiv preprint arXiv:1701.07056* (2017).
- [10] M. Hermanns, I. Kimchi, and J. Knolle, Physics of the Kitaev Model: Fractionalization, Dynamic Correlations, and Material Connections, *Annual Review of Condensed Matter Physics* **9**, 17 (2018).
- [11] H. Takagi, T. Takayama, G. Jackeli, G. Khaliullin, and S. E. Nagler, Concept and realization of Kitaev quantum spin liquids, *Nature Reviews Physics* **1**, 264 (2019).
- [12] L. Janssen and M. Vojta, Heisenberg–Kitaev physics in magnetic fields, *Journal of Physics: Condensed Matter* **31**, 423002 (2019).
- [13] Y. Motome and J. Nasu, Hunting majorana fermions in kitaev magnets, *Journal of the Physical Society of Japan* **89**, 012002 (2020).
- [14] I. Dzyaloshinsky, A thermodynamic theory of “weak” ferromagnetism of antiferromagnetics, *Journal of Physics and Chemistry of Solids* **4**, 241 (1958).
- [15] T. Moriya, Anisotropic Superexchange Interaction and Weak Ferromagnetism, *Phys. Rev.* **120**, 91 (1960).
- [16] S. Muhlbauer, B. Binz, F. Jonietz, C. Pfleiderer, A. Rosch, A. Neubauer, R. Georgii, and P. Boni, Skyrmion Lattice in a Chiral Magnet, *Science* **323**, 915 (2009).
- [17] X. Z. Yu, Y. Onose, N. Kanazawa, J. H. Park, J. H. Han, Y. Matsui, N. Nagaosa, and Y. Tokura, Real-space observation of a two-dimensional skyrmion crystal, *Nature* **465**, 901 (2010).
- [18] S. Seki, X. Z. Yu, S. Ishiwata, and Y. Tokura, Observation of Skyrmions in a Multiferroic Material, *Science* **336**, 198 (2012).
- [19] I. Kézsmárki, S. Bordács, P. Milde, E. Neuber, L. M. Eng, J. S. White, H. M. Rønnow, C. D. Dewhurst, M. Mochizuki, K. Yanai, H. Nakamura, D. Ehlers, V. Tsurkan, and A. Loidl, Néel-type skyrmion lattice with confined orientation in the polar magnetic semiconductor GaV_4S_8 , *Nature Materials* **14**, 1116 (2015).
- [20] T. Kurumaji, T. Nakajima, V. Ukleev, A. Feoktystov, T.-h. Arima, K. Kakurai, and Y. Tokura, Néel-Type Skyrmion Lattice in the Tetragonal Polar Magnet VOSe_2O_5 , *Phys. Rev. Lett.* **119**, 237201 (2017).
- [21] N. Kanazawa, Y. Onose, T. Arima, D. Okuyama, K. Ohoyama, S. Wakimoto, K. Kakurai, S. Ishiwata, and Y. Tokura, Large Topological Hall Effect in a Short-Period Helimagnet MnGe , *Phys. Rev. Lett.* **106**, 156603 (2011).
- [22] T. Tanigaki, K. Shibata, N. Kanazawa, X. Yu, Y. Onose, H. S. Park, D. Shindo, and Y. Tokura, Real-Space Observation of Short-Period Cubic Lattice of Skyrmions in MnGe , *Nano Letters* **15**, 5438 (2015).
- [23] N. Kanazawa, Y. Nii, X. X. Zhang, A. S. Mishchenko, G. D. Filippis, F. Kagawa, Y. Iwasa, N. Nagaosa, and Y. Tokura, Critical phenomena of emergent magnetic monopoles in a chiral magnet, *Nature Communications* **7**, 11622 (2016).
- [24] Y. Fujishiro, N. Kanazawa, T. Nakajima, X. Z. Yu, K. Ohishi, Y. Kawamura, K. Kakurai, T. Arima, H. Mitamura, A. Miyake, K. Akiba, M. Tokunaga, A. Matsuo, K. Kindo, T. Koretsune, R. Arita, and Y. Tokura, Topological transitions among skyrmion- and hedgehog-lattice states in cubic chiral magnets, *Nature Communications* **10**, 1059 (2019).
- [25] Y. Togawa, T. Koyama, K. Takayanagi, S. Mori, Y. Kousaka, J. Akimitsu, S. Nishihara, K. Inoue, A. S. Ovchinnikov, and J. Kishine, Chiral Magnetic Soliton Lattice on a Chiral Helimagnet, *Phys. Rev. Lett.* **108**, 107202 (2012).
- [26] J. ichiro Kishine and A. Ovchinnikov, Theory of Monoaxial Chiral Helimagnet, in *Solid State Physics* (Elsevier, 2015) pp. 1–130.
- [27] Y. Togawa, Y. Kousaka, K. Inoue, and J. ichiro Kishine, Symmetry, Structure, and Dynamics of Monoaxial Chiral Magnets, *Journal of the Physical Society of Japan* **85**, 112001 (2016).
- [28] N. Nagaosa and Y. Tokura, Emergent electromagnetism in solids, *Physica Scripta* **T146**, 014020 (2012).
- [29] A. Kitaev, Anyons in an exactly solved model and beyond, *Annals of Physics* **321**, 2 (2006).
- [30] G. Baskaran, S. Mandal, and R. Shankar, Exact Results for Spin Dynamics and Fractionalization in the Kitaev Model, *Phys. Rev. Lett.* **98**, 247201 (2007).
- [31] G. Jackeli and G. Khaliullin, Mott Insulators in the Strong Spin-Orbit Coupling Limit: From Heisenberg to a Quantum Compass and Kitaev Models, *Phys. Rev. Lett.* **102**, 017205 (2009).
- [32] J. Knolle, D. L. Kovrizhin, J. T. Chalker, and R. Moessner, Dynamics of a Two-Dimensional Quantum Spin Liquid: Signatures of Emergent Majorana Fermions and Fluxes, *Phys. Rev. Lett.* **112**, 207203 (2014).
- [33] Y. Yamaji, Y. Nomura, M. Kurita, R. Arita, and M. Imada, First-Principles Study of the Honeycomb-Lattice Iridates Na_2IrO_3 in the Presence of Strong Spin-Orbit Interaction and Electron Correlations, *Phys. Rev. Lett.* **113**, 107201 (2014).

- [34] J. Nasu, M. Udagawa, and Y. Motome, Thermal fractionalization of quantum spins in a Kitaev model: Temperature-linear specific heat and coherent transport of Majorana fermions, *Phys. Rev. B* **92**, 115122 (2015).
- [35] K. O'Brien, M. Hermanns, and S. Trebst, Classification of gapless F_2 spin liquids in three-dimensional kitaev models, *Phys. Rev. B* **93**, 085101 (2016).
- [36] N. Romming, C. Hanneken, M. Menzel, J. E. Bickel, B. Wolter, K. von Bergmann, A. Kubetzka, and R. Wiesendanger, Writing and Deleting Single Magnetic Skyrmions, *Science* **341**, 636 (2013).
- [37] P.-J. Hsu, A. Kubetzka, A. Finco, N. Romming, K. von Bergmann, and R. Wiesendanger, Electric-field-driven switching of individual magnetic skyrmions, *Nature Nanotechnology* **12**, 123 (2016).
- [38] J. Matsuno, N. Ogawa, K. Yasuda, F. Kagawa, W. Koshihara, N. Nagaosa, Y. Tokura, and M. Kawasaki, Interface-driven topological hall effect in SrRuO₃-SrIrO₃ bilayer, *Science Advances* **2**, e1600304 (2016).
- [39] S. I. Vishkayi, Z. Torbatian, A. Qaiumzadeh, and R. Asgari, Strain and electric-field control of spin-spin interactions in monolayer CrI₃, *Phys. Rev. Materials* **4**, 094004 (2020).
- [40] C.-K. Li, X.-P. Yao, and G. Chen, Writing and deleting skyrmions with electric fields in a multiferroic heterostructure, *Phys. Rev. Research* **3**, L012026 (2021).
- [41] M. Kanega, T. N. Ikeda, and M. Sato, Linear and nonlinear optical responses in kitaev spin liquids, *Phys. Rev. Research* **3**, L032024 (2021).
- [42] Y. Zhang, J. Liu, Y. Dong, S. Wu, J. Zhang, J. Wang, J. Lu, A. Rückriegel, H. Wang, R. Duine, H. Yu, Z. Luo, K. Shen, and J. Zhang, Strain-driven dzyaloshinskii-moriya interaction for room-temperature magnetic skyrmions, *Phys. Rev. Lett.* **127**, 117204 (2021).
- [43] M. Mochizuki, Spin-Wave Modes and Their Intense Excitation Effects in Skyrmion Crystals, *Phys. Rev. Lett.* **108**, 017601 (2012).
- [44] S. Seki and M. Mochizuki, *Skyrmions in magnetic materials* (Springer, 2016).
- [45] T. Kimura, T. Goto, H. Shintani, K. Ishizuka, T. Arima, and Y. Tokura, Magnetic control of ferroelectric polarization, *Nature* **426**, 55 (2003).
- [46] H. Katsura, N. Nagaosa, and A. V. Balatsky, Spin Current and Magnetoelectric Effect in Noncollinear Magnets, *Phys. Rev. Lett.* **95**, 057205 (2005).
- [47] M. Mostovoy, Ferroelectricity in Spiral Magnets, *Phys. Rev. Lett.* **96**, 067601 (2006).
- [48] I. A. Sergienko and E. Dagotto, Role of the Dzyaloshinskii-Moriya interaction in multiferroic perovskites, *Phys. Rev. B* **73**, 094434 (2006).
- [49] S.-W. Cheong and M. Mostovoy, Multiferroics: a magnetic twist for ferroelectricity, *Nature Materials* **6**, 13 (2007).
- [50] T. Arima, Ferroelectricity Induced by Proper-Screw Type Magnetic Order, *Journal of the Physical Society of Japan* **76**, 073702 (2007).
- [51] Y. Tokura, S. Seki, and N. Nagaosa, Multiferroics of spin origin, *Reports on Progress in Physics* **77**, 076501 (2014).
- [52] S. Z. Bisri, S. Shimizu, M. Nakano, and Y. Iwasa, Endeavor of Iontronics: From Fundamentals to Applications of Ion-Controlled Electronics, *Advanced Materials* **29**, 1607054 (2017).
- [53] K. Ueno, H. Shimotani, H. Yuan, J. Ye, M. Kawasaki, and Y. Iwasa, Field-Induced Superconductivity in Electric Double Layer Transistors, *Journal of the Physical Society of Japan* **83**, 032001 (2014).
- [54] G. Chen, T. Ma, A. T. N'Diaye, H. Kwon, C. Won, Y. Wu, and A. K. Schmid, Tailoring the chirality of magnetic domain walls by interface engineering, *Nature Communications* **4**, 10.1038/ncomms3671 (2013).
- [55] See Supplemental Material for details about technical calculations of microscopic parameters.
- [56] J. Chen, *Introduction to Scanning Tunneling Microscopy Third Edition*, Vol. 69 (Oxford University Press, USA, 2021).
- [57] N. P. Magtoto, C. Niu, B. M. Ekstrom, S. Addepalli, and J. A. Kelber, Dielectric breakdown of ultrathin aluminum oxide films induced by scanning tunneling microscopy, *Applied Physics Letters* **77**, 2228 (2000).
- [58] K. Takasan and M. Sato, Control of magnetic and topological orders with a DC electric field, *Phys. Rev. B* **100**, 060408 (2019).
- [59] S. C. Furuya, K. Takasan, and M. Sato, Control of superexchange interactions with DC electric fields, *Phys. Rev. Research* **3**, 033066 (2021).
- [60] H. Eskes and J. H. Jefferson, Superexchange in the cuprates, *Phys. Rev. B* **48**, 9788 (1993).
- [61] G. Khaliullin, Orbital Order and Fluctuations in Mott Insulators, *Progress of Theoretical Physics Supplement* **160**, 155 (2005).
- [62] H. Liu and G. Khaliullin, Pseudospin exchange interactions in d^7 cobalt compounds: Possible realization of the kitaev model, *Phys. Rev. B* **97**, 014407 (2018).
- [63] Y. Sugita, Y. Kato, and Y. Motome, Antiferromagnetic kitaev interactions in polar spin-orbit mott insulators, *Phys. Rev. B* **101**, 100410 (2020).
- [64] S. Sugano, Y. Tanabe, and H. Kamimura, *Multiplets of transition-metal ions in crystals* (Academic Press, New York, 1970).
- [65] B. J. Kim, H. Jin, S. J. Moon, J.-Y. Kim, B.-G. Park, C. S. Leem, J. Yu, T. W. Noh, C. Kim, S.-J. Oh, J.-H. Park, V. Durairaj, G. Cao, and E. Rotenberg, Novel $J_{\text{eff}} = 1/2$ Mott State Induced by Relativistic Spin-Orbit Coupling in Sr₂IrO₄, *Phys. Rev. Lett.* **101**, 076402 (2008).
- [66] Y. Onodera and M. Okazaki, Tables of Basis Functions for Double Point Groups, *Journal of the Physical Society of Japan* **21**, 2400 (1966).
- [67] T. Takayama, J. Chaloupka, A. Smerald, G. Khaliullin, and H. Takagi, Spin-Orbit-Entangled Electronic Phases in 4d and 5d Transition-Metal Compounds, *Journal of the Physical Society of Japan* **90**, 062001 (2021).
- [68] J. B. Goodenough, Theory of the Role of Covalence in the Perovskite-Type Manganites [La, M(II)]MnO₃, *Phys. Rev.* **100**, 564 (1955).
- [69] J. Kanamori, Theory of the Magnetic Properties of Ferrous and Cobaltous Oxides, I, *Progress of Theoretical Physics* **17**, 177 (1957).
- [70] J. Kanamori, Theory of the Magnetic Properties of Ferrous and Cobaltous Oxides, II, *Progress of Theoretical Physics* **17**, 197 (1957).
- [71] D. Takikawa and S. Fujimoto, Impact of off-diagonal exchange interactions on the kitaev spin-liquid state of α -ruCl₃, *Phys. Rev. B* **99**, 224409 (2019).
- [72] D. Takikawa and S. Fujimoto, Topological phase transition to abelian anyon phases due to off-diagonal exchange

- interaction in the kitaev spin liquid state, *Phys. Rev. B* **102**, 174414 (2020).
- [73] A. Banerjee, C. A. Bridges, J.-Q. Yan, A. A. Aczel, L. Li, M. B. Stone, G. E. Granroth, M. D. Lumsden, Y. Yiu, J. Knolle, S. Bhattacharjee, D. L. Kovrizhin, R. Moessner, D. A. Tennant, D. G. Mandrus, and S. E. Nagler, Proximate Kitaev quantum spin liquid behaviour in a honeycomb magnet, *Nature Materials* **15**, 733 (2016).
- [74] R. Yadav, N. A. Bogdanov, V. M. Katukuri, S. Nishimoto, J. van den Brink, and L. Hozoi, Kitaev exchange and field-induced quantum spin-liquid states in honeycomb α -RuCl₃, *Scientific Reports* **6**, 10.1038/srep37925 (2016).
- [75] A. Glamazda, P. Lemmens, S.-H. Do, Y. S. Kwon, and K.-Y. Choi, Relation between Kitaev magnetism and structure in α -RuCl₃, *Phys. Rev. B* **95**, 174429 (2017).
- [76] A. U. B. Wolter, L. T. Corredor, L. Janssen, K. Nenkov, S. Schönecker, S.-H. Do, K.-Y. Choi, R. Albrecht, J. Hunger, T. Doert, M. Vojta, and B. Büchner, Field-induced quantum criticality in the Kitaev system α -RuCl₃, *Phys. Rev. B* **96**, 041405 (2017).
- [77] Y. Kasahara, K. Sugii, T. Ohnishi, M. Shimozawa, M. Yamashita, N. Kurita, H. Tanaka, J. Nasu, Y. Motome, T. Shibauchi, and Y. Matsuda, Unusual Thermal Hall Effect in a Kitaev Spin Liquid Candidate α -RuCl₃, *Phys. Rev. Lett.* **120**, 217205 (2018).
- [78] D. Wulferding, Y. Choi, S.-H. Do, C. H. Lee, P. Lemmens, C. Faugeras, Y. Gallais, and K.-Y. Choi, Magnon bound states versus anyonic Majorana excitations in the Kitaev honeycomb magnet α -RuCl₃, *Nature Communications* **11**, 10.1038/s41467-020-15370-1 (2020).
- [79] M. Yamashita, J. Gouchi, Y. Uwatoko, N. Kurita, and H. Tanaka, Sample dependence of half-integer quantized thermal hall effect in the kitaev spin-liquid candidate α -rucl₃, *Phys. Rev. B* **102**, 220404 (2020).
- [80] H. Suzuki, H. Liu, J. Bertinshaw, K. Ueda, H. Kim, S. Laha, D. Weber, Z. Yang, L. Wang, H. Takahashi, K. Fürsich, M. Minola, B. V. Lotsch, B. J. Kim, H. Yavas, M. Daghofer, J. Chaloupka, G. Khaliullin, H. Gretarsson, and B. Keimer, Proximate ferromagnetic state in the Kitaev model material α -RuCl₃, *Nature Communications* **12**, 10.1038/s41467-021-24722-4 (2021).
- [81] A. Ralko and J. Merino, Novel chiral quantum spin liquids in kitaev magnets, *Phys. Rev. Lett.* **124**, 217203 (2020).
- [82] H. Min, J. E. Hill, N. A. Sinitsyn, B. R. Sahu, L. Kleinman, and A. H. MacDonald, Intrinsic and Rashba spin-orbit interactions in graphene sheets, *Phys. Rev. B* **74**, 165310 (2006).
- [83] A. D. Caviglia, M. Gabay, S. Gariglio, N. Reyren, C. Cancellieri, and J.-M. Triscone, Tunable Rashba Spin-Orbit Interaction at Oxide Interfaces, *Phys. Rev. Lett.* **104**, 126803 (2010).
- [84] C. R. Ast, J. Henk, A. Ernst, L. Moreschini, M. C. Falub, D. Pacilé, P. Bruno, K. Kern, and M. Grioni, Giant spin splitting through surface alloying, *Phys. Rev. Lett.* **98**, 186807 (2007).
- [85] K. V. Shanavas and S. Satpathy, Electric field tuning of the rashba effect in the polar perovskite structures, *Phys. Rev. Lett.* **112**, 086802 (2014).
- [86] K. Shimizu, S. Okumura, Y. Kato, and Y. Motome, Spin moiré engineering of topological magnetism and emergent electromagnetic fields, *Phys. Rev. B* **103**, 184421 (2021).
- [87] H. Ohno, D. Chiba, F. Matsukura, T. Omiya, E. Abe, T. Dietl, Y. Ohno, and K. Ohtani, Electric-field control of ferromagnetism, *Nature* **408**, 944 (2000).
- [88] F. Matsukura, Y. Tokura, and H. Ohno, Control of magnetism by electric fields, *Nature Nanotechnology* **10**, 209 (2015).
- [89] L. Chen, F. Matsukura, and H. Ohno, Electric-Field Modulation of Damping Constant in a Ferromagnetic Semiconductor (Ga,Mn)As, *Phys. Rev. Lett.* **115**, 057204 (2015).
- [90] S. Jiang, J. Shan, and K. F. Mak, Electric-field switching of two-dimensional van der Waals magnets, *Nature Materials* **17**, 406 (2018).
- [91] B. Huang, G. Clark, D. R. Klein, D. MacNeill, E. Navarro-Moratalla, K. L. Seyler, N. Wilson, M. A. McGuire, D. H. Cobden, D. Xiao, W. Yao, P. Jarillo-Herrero, and X. Xu, Electrical control of 2D magnetism in bilayer CrI₃, *Nature Nanotechnology* **13**, 544 (2018).
- [92] X. Chen, X. Zhou, R. Cheng, C. Song, J. Zhang, Y. Wu, Y. Ba, H. Li, Y. Sun, Y. You, Y. Zhao, and F. Pan, Electric field control of Néel spin-orbit torque in an antiferromagnet, *Nature Materials* **18**, 931 (2019).
- [93] C. Xu, P. Chen, H. Tan, Y. Yang, H. Xiang, and L. Bellaiche, Electric-Field Switching of Magnetic Topological Charge in Type-I Multiferroics, *Phys. Rev. Lett.* **125**, 037203 (2020).
- [94] H. Hirori, A. Doi, F. Blanchard, and K. Tanaka, Single-cycle terahertz pulses with amplitudes exceeding 1 MV/cm generated by optical rectification in LiNbO₃, *Applied Physics Letters* **98**, 091106 (2011).
- [95] Y. Mukai, H. Hirori, T. Yamamoto, H. Kageyama, and K. Tanaka, Nonlinear magnetization dynamics of antiferromagnetic spin resonance induced by intense terahertz magnetic field, *New Journal of Physics* **18**, 013045 (2016).
- [96] D. Nicoletti and A. Cavalleri, Nonlinear light-matter interaction at terahertz frequencies, *Advances in Optics and Photonics* **8**, 401 (2016).
- [97] J. A. Fülöp, S. Tzortzakis, and T. Kampfrath, Laser-Driven Strong-Field Terahertz Sources, *Advanced Optical Materials* **8**, 1900681 (2019).
- [98] M. Sato, S. Takayoshi, and T. Oka, Laser-Driven Multiferroics and Ultrafast Spin Current Generation, *Phys. Rev. Lett.* **117**, 147202 (2016).
- [99] M. Sato, Floquet theory and ultrafast control of magnetism, Chirality, Magnetism and Magnetoelectricity: Separate Phenomena and Joint Effects in Metamaterial Structures **138**, 265 (2021).